Machine Learning-Based Summer Crops Mapping Using Sentinel-1 and Sentinel-2 Images

Saeideh Maleki, Nicolas Baghdadi, Hassan Bazzi, Cassio Fraga Dantas, Dino Ienco, Yasser Nasrallah, Sami Najem

remote sensing

MDPI

Article

Machine Learning-Based Summer Crops Mapping Using Sentinel-1 and Sentinel-2 Images

Saeideh Maleki [1], Nicolas Baghdadi [1,*], Hassan Bazzi [1], Cassio Fraga Dantas [1,2], Dino Ienco [1,2], Yasser Nasrallah [1] and Sami Najem [1]

[1] Territoires, Environnement, Télédétection et Information Spatiale (TETIS), University of Montpellier, Paris Institute of Technology for Life, Food and Environmental Sciences (AgroParisTech), French Agricultural Research Centre for International Development (CIRAD)/French National Center for Scientific Research (CNRS)/French National Research Institute for Agriculture, Food, and the Environment (INRAE), 34093 Montpellier, France; saeideh.maleki-najafabadi@inrae.fr (S.M.); hassan.bazzi@agroparistech.fr (H.B.); cassio.fraga-dantas@inrae.fr (C.F.D.); dino.ienco@inrae.fr (D.I.); yasser.nasrallah@inrae.fr (Y.N.); sami.najem@inrae.fr (S.N.)

[2] National Institute for Research in Digital Science and Technology (INRIA), Université de Montpellier, Antenne INRIA de l'Université de Montpellier, 34090 Montpellier, France

* Correspondence: nicolas.baghdadi@inrae.fr

Abstract: Accurate crop type mapping using satellite imagery is crucial for food security, yet accurately distinguishing between crops with similar spectral signatures is challenging. This study assessed the performance of Sentinel-2 (S2) time series (spectral bands and vegetation indices), Sentinel-1 (S1) time series (backscattering coefficients and polarimetric parameters), alongside phenological features derived from both S1 and S2 time series (harmonic coefficients and median features), for classifying sunflower, soybean, and maize. Random Forest (RF), Multi-Layer Perceptron (MLP), and XGBoost classifiers were applied across various dataset configurations and train-test splits over two study sites and years in France. Additionally, the InceptionTime classifier, specifically designed for time series data, was tested exclusively with time series datasets to compare its performance against the three general machine learning algorithms (RF, XGBoost, and MLP). The results showed that XGBoost outperformed RF and MLP in classifying the three crops. The optimal dataset for mapping all three crops combined S1 backscattering coefficients with S2 vegetation indices, with comparable results between phenological features and time series data (mean F1 scores of 89.9% for sunflower, 76.6% for soybean, and 91.1% for maize). However, when using individual satellite sensors, S1 phenological features and time series outperformed S2 for sunflower, while S2 was superior for soybean and maize. Both phenological features and time series data produced close mean F1 scores across spatial, temporal, and spatiotemporal transfer scenarios, though median features dataset was the best choice for spatiotemporal transfer. Polarimetric S1 data did not yield effective results. The InceptionTime classifier further improved classification accuracy over XGBoost for all crops, with the degree of improvement varying by crop and dataset (the highest mean F1 scores of 90.6% for sunflower, 86.0% for soybean, and 93.5% for maize).

Keywords: Random Forest; Multi-Layer Perceptron; XGBoost; InceptionTime; S1 backscattering coefficient; S1 polarimetric parameters; S2 vegetation indices

Citation: Maleki, S.; Baghdadi, N.; Bazzi, H.; Dantas, C.F.; Ienco, D.; Nasrallah, Y.; Najem, S. Machine Learning-Based Summer Crops Mapping Using Sentinel-1 and Sentinel-2 Images. *Remote Sens.* **2024**, *16*, 4548. https://doi.org/10.3390/rs16234548

Academic Editor: Xijian Fan

Received: 19 October 2024
Revised: 18 November 2024
Accepted: 2 December 2024
Published: 4 December 2024

1. Introduction

Monitoring agricultural systems has become increasingly crucial in addressing global challenges such as climate change, biodiversity loss, population growth, and the growing demand for agricultural products [1–3]. Accurate mapping of summer crops is essential not only for ensuring food security but also for managing water resources, as many of these crops rely on irrigation. With climate change intensifying pressure on water availability, precise agricultural maps are vital for optimizing water usage and tracking water consumption [4].

Remote sensing data serves as a key tool for large-scale monitoring of land surfaces and crop mapping. Optical imagery is particularly valuable for crop mapping because it captures detailed information about crop growth and health through multiple spectral bands that are sensitive to different stages of plant development [5–10]. However, optical data have limitations, particularly in regions with frequent cloud cover or haze, which can disrupt continuous data collection over time. In addition, since optical imagery often targets key stages of crop growth, it is more susceptible to weather-related disruptions during these stages [1,11]. In contrast, radar data are particularly advantageous in regions with frequent cloud cover, where optical sensors face significant challenges. Radar data can also penetrate vegetation and provide structural details that are especially useful for mapping crops like sunflowers [12]. However, studies have shown that, in general, radar data tends to provide lower classification accuracy compared to optical data [5,13,14]. Most studies using radar data focus on backscattering coefficients (VV, VH, and the VV/VH ratio), which offer valuable information for crop classification [15–17]. However, few studies have explored the use of radar polarimetric parameters. This is largely due to the fact that Sentinel-1 (S1) images, which are free accessible radar images, are not fully polarimetric, and the polarimetric parameters derived from dual-polarization data are less informative compared to those obtained from fully polarimetric synthetic aperture radar (SAR). Additionally, calculating polarimetric parameters can be time consuming, especially when dealing with time series data across multiple study sites or phenological cycles. However, certain polarimetric parameters, which capture backscattering mechanisms and wave interactions, may be highly sensitive to changes in crop phenology, offering valuable insights into crop growth stages [18,19].

Despite the strengths of both optical and radar imagery, crop type mapping remains challenging due to the high spectral, spatial, and temporal variability observed throughout the growing season [20]. Different crops often exhibit similar spectral and spatial characteristics, as seen in the case of mapping soybean, maize, and sunflower [21]. Additionally, the same crop can display varying traits under different environmental conditions [22]. These similarities between different crops, combined with the variability of a single crop in diverse conditions, result in high inter-class similarity and low intra-class distinction, making accurate crop classification a complex task [23]. To address this complexity, numerous studies tended to enhance classification accuracy while minimizing data redundancy and processing time in crop mapping research [22,24,25]. Several approaches have been applied to improve crop mapping. One approach is the combination of optical and radar data, which has proven effective in enhancing crop classification [5,25,26]. For example, Valero et al. [8] achieved a 6% higher accuracy in mapping five crops—sunflower, maize, rapeseed, sorghum, and straw—by combining S1 and Sentinel-2 (S2) images, compared to using S2 images alone. Demarez et al. [27] demonstrated that the combined use of S1, Landsat, and SRTM data resulted in a 5% improvement in classification accuracy of the irrigated crops compared to using each type of data separately. Another approach to improve crop mapping involves the use of phenological features, such as harmonic coefficients and median features derived from satellite data, which have also shown promise [17,28]. Qadir et al. [12] achieved an F1 score of 97% in detecting sunflower by using a training and testing dataset from the same site in Ukraine, based on median features extracted from S1 images. Wang et al. [28] reported an R^2 value greater than 0.85 for mapping maize and soybean across several states in the USA. Furthermore, to improve crop mapping, Artificial Intelligence (AI) algorithms have gained more interest in recent years [13,29,30], offering significant improvements in crop classification. With their capacity to handle complex and large datasets, these algorithms have proven effective in addressing challenges such as high inter-class similarity and low intra-class distinction, enabling accurate mapping of multiple crop types across large and diverse regions [31–33]. Furthermore, their ability to assess the importance of inputs makes them particularly valuable in time series analysis using multiple features [29]. Among AI algorithms, machine learning algorithms such as XGBoost, Random Forest (RF), and Support Vector Machines (SVMs) are widely used in

crop mapping due to their user-friendly nature, low computational requirements and high accuracy in classifying crops with similar spectral and spatial characteristics, especially among summer crops [24,25]. On the other hand, deep learning (DL) methods are gaining significant interest in satellite image classification, as they can learn to perform image classification in an end-to-end manner directly from raw input data [31–33]. However, given this diversity of remote sensing products and algorithms, users of remote sensing data are often faced with the challenge of selecting the most appropriate dataset approaches and algorithms, while decision makers are primarily concerned with comparing the results of these approaches and algorithms.

This paper aims to discover both effective datasets and classifiers for mapping summer crops with similar spectral and spatial characteristics. It compares the effectiveness of various classifiers and satellite sensors in mapping sunflower, maize, and soybean—three key summer crops. Maize is one of the world's major crops, with the European Union being the fourth-largest producer [34]. France is the leading producer of maize in Europe, accounting for nearly 20% of the continent's maize production in 2023 [35]. Sunflower and soybean are also major oilseed crops globally, contributing 60% and 20%, respectively, to the world's oilseed consumption [36]. Previous studies have shown that achieving high-accuracy maps for soybean, maize, and sunflower crops is challenging due to their similar spectral characteristics, especially in their early growth stages [37,38]. This similarity makes it hard to distinguish between them [6,39]. Additionally, summer crops are sensitive to environmental stressors, such as drought, which can alter their optical spectral or radar backscatter responses [40]. These variations further complicate classification, as stressed crops may resemble other crops. So, we will identify which dataset and classifiers can efficiently address these challenges to produce reliable maps. Furthermore, since limitations in ground data availability across regions and times pose challenges in crop mapping [41,42], we conducted classifications using training data from one study site and year to create maps for different study sites and years across three types of transfer scenarios: spatial, temporal, and spatiotemporal. This comprehensive approach can guide future users in selecting the most suitable datasets and algorithms for accurate crop mapping across varying conditions.

To achieve the aforementioned objectives through a comprehensive assessment of different satellite products, we present mapping approaches of sunflower, maize, and soybean using time series data from S2 spectral bands, S2 vegetation indices, S1 radar backscattering coefficients, and S1 polarimetric parameters, alongside phenological features such as harmonic coefficients and median features extracted from S1 and S2 time series data. RF, Multi-Layer Perceptron (MLP), and XGBoost classifiers were used to classify datasets across six combinations of study sites and years from Tarbes 2020, Tarbes 2021, and Dijon 2020, all located in France. Additionally, the InceptionTime classifier, specifically designed for time series data, was tested exclusively with time series datasets to compare its performance against the three general machine learning algorithms (RF, XGBoost, and MLP). The main contribution of this paper is its comprehensive comparison of different data configurations (S1 and S2) and high-performing classifiers (RF, XGBoost, MLP, and InceptionTime) for crop classification. Our study analyzes both optical and radar time series data—including reflectance, vegetation indices, radar backscatter, and S1 polarimetric parameters—using timeseries and phenological metrics like median features and harmonic coefficients as inputs for the classifiers. Additionally, this paper explores the use of S1 polarimetric data for crop classification. Since there is limited research on how well S1 polarimetric data can distinguish crops with similar spectral features, our study provides important insights into its potential.

2. Materials and Methods

2.1. Study Site

The study is carried out in Tarbes in the southwest and Dijon in the northeast of France. This choice was made to consider possible differences in crop growth cycles between the north and south of France. Dijon is located in the Côte-d'Or department of the

Bourgogne-Franche-Comté region. Tarbes is located in the Hautes-Pyrénées department of the Midi-Pyrénées region. Dijon has an annual average temperature of 12.5 °C and annual rainfall of about 743 mm, while Tarbes has a higher annual average temperature of 13.7 °C and an annual rainfall of about 1081 mm [43], making it both wetter and warmer than Dijon. The study focuses on the mapping of maize fields, a major agricultural crop in France, along with sunflower and soybean, both important oilseed sources. Figure 1a shows the location of our study sites and the proportion of these three summer crops within the total cultivated area in Tarbes (2020 and 2021) and Dijon (2020). In France, maize planting begins in April and is harvested in October, soybean planting starts in May and is harvested in October, and sunflower planting begins in April and is harvested in September (Figure 1b) [44].

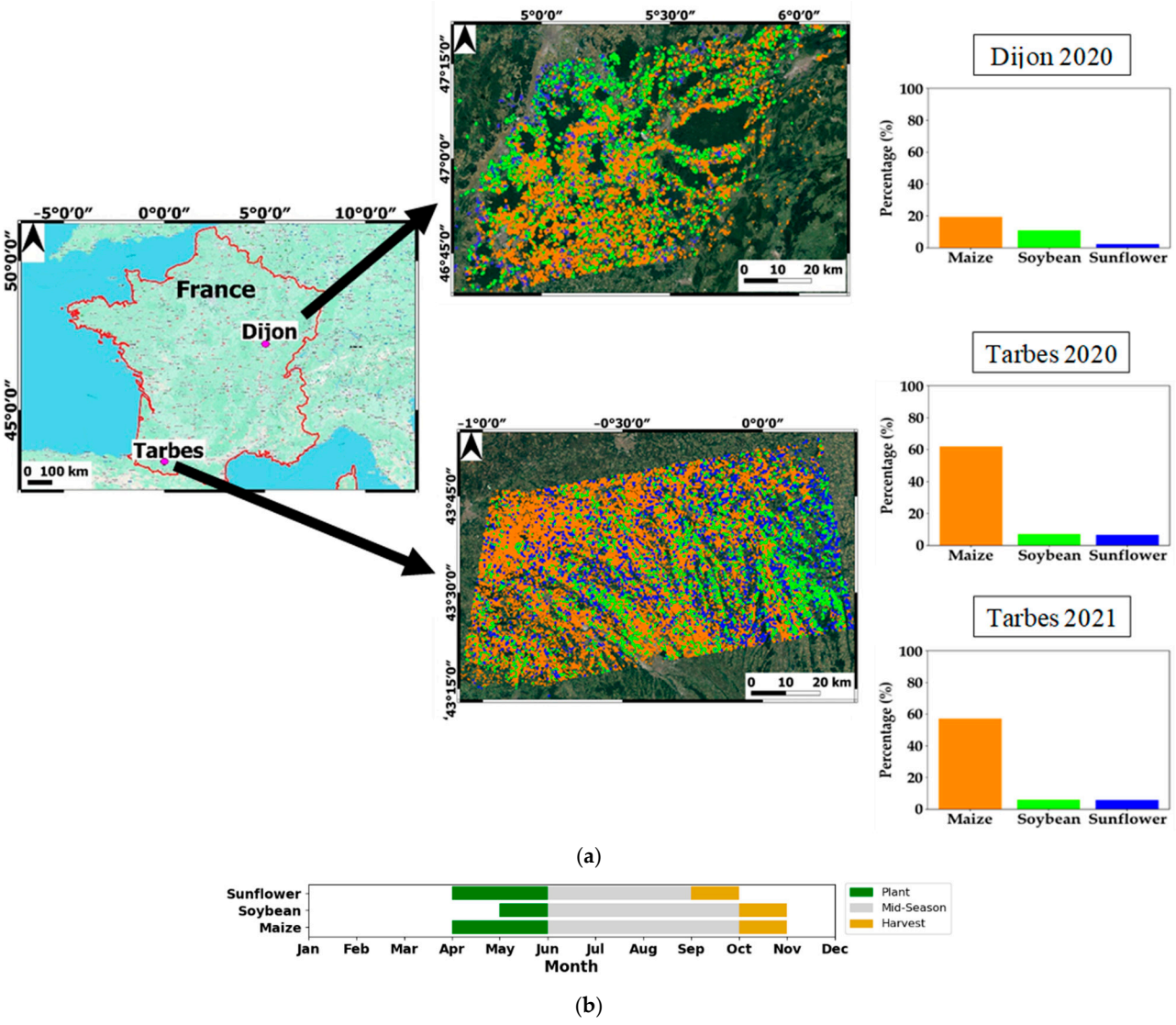

Figure 1. (**a**) Location of our study sites and the portion of cropped area for the main three summer crops in the study years. (**b**) Dates of sowing and harvest of sunflower, soybean, and maize in France.

2.2. Data

2.2.1. Ground Data

We extracted ground data from the French Graphic Parcel Registry (RPG), which provides detailed information on the boundaries, crop types, and sizes of agricultural fields declared by farmers across France. The complete database is publicly accessible

at https://www.data.gouv.fr/en/datasets/registre-parcellaire-graphique-rpg-contours-des-parcelles-et-ilots-culturaux-et-leur-groupe-de-cultures-majoritaire, (accessed on 3 February 2024). Table 1 shows the number of reference fields in each dataset that were used as ground data for the three summer crops (sunflower, soybean, and maize).

Table 1. Number of fields for the three selected summer crops in Dijon (2020) and Tarbes (2020 and 2021).

Study Site/Year	Crop Type	Number of Reference Fields
Dijon 2020	Sunflower	853
	Soybean	4630
	Maize	8344
Tarbes 2020	Sunflower	4807
	Soybean	5293
	Maize	47,015
Tarbes 2021	Sunflower	5124
	Soybean	5554
	Maize	53,256

2.2.2. Sentinel-2 Data

In this study, we used Sentinel-2 (S2) Level-2A (L2A) products from the Sentinel-2A and Sentinel-2B satellites, available through the Google Earth Engine (GEE) [45]. The L2A products represent bottom-of-atmosphere (BOA) reflectance, which has undergone atmospheric correction to remove the effects of gasses and aerosols in the atmosphere, using ESA's Sen2Cor processor [25]. This correction ensures that the reflectance values more accurately represent surface conditions. Additionally, terrain correction was applied to minimize topographic effects on reflectance. For cloud masking, we used the quality assessment band (QA60) to filter out cloudy and shadowed pixels, ensuring that only clear observations contributed to the analysis. This step is crucial to enhance the reliability of the time series and prevent cloud contamination in vegetation indices and other analyses. The potential gaps resulting from clouds were consequently mitigated using a gap-filling technique consisting of fitting and resampling the data. The Sav-Gol function was used for fitting with a window length of 3 [17]. The data were resampled to one point every 10 days, ensuring that there was enough repeatability to follow the rapid development of the summer crop, especially during its vegetative growth stage. We created the S2 time series for Tarbes (2020 and 2021) and Dijon (2020), covering the entire growth period of the three selected summer crops: sunflower, soybean, and maize (1 April to 1 December). Our S2 dataset contained 41 images in 12 bands for each study site/year. This study was conducted at the field level, so for each band, the mean pixel value was calculated for each field.

In addition to spectral bands, thirteen vegetation indices commonly cited in crop mapping studies were derived from S2 datasets for each study site and year. Table 2 provides a summary of these indices along with their respective equations, utilizing S2 bands.

Table 2. List of vegetation indices calculated from S2 datasets. NIR: Near-infrared, SWIR: Shortwave infrared.

Vegetation Index	Equation	Applications	Reference
Normalized Difference Vegetation Index (NDVI)	$(NIR - R)/(NIR + R)$	Biomass, yield, disease, soil moisture, water stress	[46]
Land Surface Water Index (LSWI)	$(NIR - SWIR1)/(NIR + SWIR1)$	Monitoring crop water stress	[47]
Normalized Difference Red Edge Index (NDRE)	$(Rededge2 - Rededge1)/(Rededge2 + Rededge1)$	Crop yield, biomass, disease	[48]
Red-Edge Spectral Indices (RESI)	$(Rededge3 + Rededge2 - Rededge1)/(Rededge3 + Rededge2 + Rededge1)$	Discriminating between different types of vegetation, monitoring crop stress, chlorophyll content, senescence	[49]
Normalized Difference Senescent Vegetation Index (NDSVI)	$(SWIR1 - Red)/(SWIR1 + Red)$	Monitor crop aging or stress	[50]
Modified Crop Residue Cover (MODCRC)	$(SWIR1 - Green)/(SWIR1 + Green)$	Crop residue, classify crops based on the level of residue cover	[51]
Chlorophyll Index Green (CIgreen)	$(NIR/Green) - 1$	Crop stress, growth anomalies	[49]
Chlorophyll Index Red Edge (CI red_edge)	$(NIR/Rededge3) - 1$	Crop stress, growth anomalies	[49]
Normalized Difference Water Index (NDWI)	$(Green - NIR)/(Green + NIR)$	Vegetation water content	[52]
Red Edge Normalized Difference Vegetation Index (RENDVI)	$(NIR - Rededge2)/(NIR + Rededge2)$	Yield, irrigation management, disease	[53]
Green Normalized Difference Vegetation Index (GNDVI)	$(NIR - Green)/(NIR + Green)$	Water stress, yield, biomas, disease	[48]
Enhanced Vegetation Index (EVI)	$2.5((NIR - Red)/((NIR + 6Red - 7.5Blue) + 1))$	Disease, biomass	[54]
Modified Soil Adjusted Vegetation Index (MSAVI)	$\frac{((2NIR+1) - \sqrt{((2NIR+1)^2 - 8(NIR - Red))})}{2}$	Biomass, crop yield, chlorophyll content	[55]

2.2.3. Sentinel-1 Data

In this study, Sentinel-1A (S1A) and Sentinel-1B (S1B) satellite images, with a combined 6-day revisit interval, were used in two types: Single Look Complex (S1_SLC) in Interferometric Wide Swath (IW) mode for polarimetric analysis and Ground Range Detected (S1-GRD) for backscatter analysis using sigma values. Both products were downloaded in dual polarization (VV and VH). One ascending and one descending orbit were selected for each study site and year. The incidence angle of S1 images across our study sites varied for Tarbes from 30° to 41° for the ascending orbit and from 34° to 44° for descending orbit. For Dijon, it varies from 35° to 44° for ascending orbit and from 30° to 39° for descending orbit. Our study sites have minimal elevation variation, resulting in a reduced influence of local incidence angle effects on backscatter values.

Sentinel-1 Backscattering Coefficients

We extracted the mean backscatter coefficients (VV and VH) for each field from Sentinel-1 Ground Range Detected (S1-GRD) images using the Google Earth Engine (GEE). These images had already undergone preprocessing, including thermal noise removal,

multi-looking, co-registration, radiometric calibration, and terrain correction [56]. Thermal noise removal was applied to reduce sensor-related noise; multi-looking was used to decrease speckle and improve image quality; and co-registration was performed to align images for accurate temporal analysis. Additionally, radiometric calibration converted raw data into backscatter values, and terrain correction was applied to adjust for topographic distortions, ensuring accurate spatial representation of surface backscatter properties.

In addition to the VV and VH polarizations, the ratio of VV and VH polarizations (VV/VH) was calculated as well as the difference between ascending and descending orbits for each polarization and for VV/VH ratio. As a result, three datasets were generated for the S1 backscattering coefficient:

- For the ascending orbit (asc), containing time series for VV_{asc}, VH_{asc}, and VV/VH_{asc};
- For the descending orbit (des), containing time series for VV_{des}, VH_{des}, and VV/VHdes;
- Both orbits, containing the two datasets mentioned above in addition to the differences between them: VV_{asc}-VV_{des}, VH_{asc}-VH_{des}, and VV/VH_{asc}-VV/VH_{des}.

Sentinel-1 Polarimetric Data

Polarimetric SAR data capture detailed information about the polarization amplitude and phase of the radar signal which can be useful for crop detection. As crops develop, there is not only an increase in radar backscatter but also a greater variability in scattering patterns, along with increased contributions from multiple or volume scattering [18]. This variability suggests that certain polarimetric parameters, which capture backscattering mechanisms and wave interactions, may be particularly sensitive to changes in crop phenology, offering valuable insights into crop growth stages. Therefore, we calculated several polarimetric parameters for this study. S1_SLC images were downloaded from NASA's Earth Observing System Data and Information System (EOSDIS, https://search.asf.alaska.edu, accessed on 11 April 2024). All preprocessing steps to derive polarimetric parameters were conducted using ESA's Sentinel Application Platform (SNAP) v.7.0.0 and PolSARpro v.6.0. These steps included applying orbit files, performing Terrain Observation with Progressive Scans (TOPS) splitting, radiometric calibration, TOPS debursting, polarimetric speckle filtering, and terrain correction. Five polarimetric parameters were used in this study, including two Stokes parameters including g0 and g1 and three Shannon entropy-based polarimetric decomposition parameters: Shannon_I, Shannon_P and Shannon. The Stokes parameters describe the scattering from a partially polarized electromagnetic field and capture all the polarimetric information [19]. The first Stokes parameter (g0) represents the total intensity of the radar backscatter, while g1 indicates the polarized part of the electromagnetic field [18]. Shannon entropy parameters measure the randomness of the scattering process [18]. Shannon entropy is computed using the covariance matrix (Equation (1)). This polarimetric parameter can be expressed as the sum of two components including Shannon_I and Shannon_P, representing randomness associated with changes in signal intensity and phase, respectively [18] (Equations (2) and (3)).

$$\text{Shannon} = \log\left(\pi^2\, e^2 \det[C_2]\right) = \text{Shannon\_I} + \text{Shannon\_P} \quad (1)$$

$$\text{Shannon\_I} = 2\log\left((\pi e \text{Tr}[C_2])/2\right) \quad (2)$$

$$\text{Shannon\_P} = \log((4\det[C_2])/(\text{Tr}\,[C_2]^2)) \quad (3)$$

where "$[C_2]$" refers to the 2 × 2 covariance matrix, "Tr" and "det" refer to the trace and determinant of the covariance matrix, respectively.

Three S1 polarimetric time series datasets were generated:

- For the ascending orbit, containing five polarimetric parameters: g0, g1, Shannon_I, Shannon_P, and Shannon
- For the descending orbit with the same polarimetric parameters
- For both ascending and descending orbits as well as the differences between them (for example: $g0_{asc}$-$g0_{des}$, $g1_{asc}$-$g1_{des}$, etc.).

To generate each S1 backscattering coefficients and S1 polarimetric time series at the field level, the mean value using all pixels in each field was used. Each time series covered the entire growth period of the summer crops in the study site, aligned with the same period as the S2 time series, from 1 April to 1 December each year. For each orbit, the S1 polarimetric parameter and S1 backscattering coefficients time series contained 41 images per study site and year. The S1 backscattering coefficients time series was generated for Tarbes in 2020 and 2021 and for Dijon in 2020 (Table 3). Given that the time required to generate polarimetric data are very high (one month per site), we chose to use the polarimetric data for the S1 polarimetric time series for Tarbes in 2021 and Dijon in 2020 (Table 3).

Table 3. S1 and S2 data used in the study, including study sites, years, and study periods.

Satellite	Time Series	Study Site/Year	Study Period (per Year)
S2	S2 bands time series S2 vegetation indices time series S1 backscattering coefficients time series	Dijon 2020, Tarbes 2020,Tarbes 2021	From 1 April to 1 December
S1	S1 polarimetric parameters time series	Dijon 2020, Tarbes 2021	

2.3. Methodology

2.3.1. Features

The study evaluated the effectiveness of free and open-access S1 radar and S2 optical data for mapping sunflower, soybean, and maize. This involved analyzing spectral bands and indices from S2, along with backscattering coefficients and polarimetric parameters from the S1 dataset (as detailed in Sections 2.2.2 and 2.2.3), as summarized in Table 4. In addition, several features were calculated from S1 and S2 time series using harmonic regression [28] and median values calculated for each phenological stage and across different seasons [12]. The flowchart of study has been presented in Figure 2.

Table 4. The time series (TS) and features employed in this study. Sh = Shannon, Sh_I = Shannon_I, Sh_P = Shannon_P.

Satellite	Time Series	Details	Features	
S2	S2 spectral bands	12 time series	B1, B2, B3, B4, B5, B6, B7, B8, B8A, B9, B11, B12	
		5 harmonic coefficients for each time series	a_1, a_2, b_1, b_2, c (Equation (4))	
		7 median features for each time series	P_1	June
			P_2	July
			P_3	August
			P_4	September
			S_1	April + May
			S_2	June + July + August
			S_3	September + October + November
	S2 vegetation indices	13 time series	LSWI, NDRE, RESI, NDSVI, MODCRC, CIgreen, CI_red_edge, NDWI, RENDVI, GNDVI, EVI, MSAVI, NDVI	
		5 harmonic coefficients for each time series	a_1, a_2, b_1, b_2, c (Equation (4))	
		7 median features for each time series	P_1, P_2, P_3, P_4, S_1, S_2, S_3	

Table 4. *Cont.*

Satellite	Time Series		Details	Features
S1	S1 backscattering coefficients	S1 ascending orbit	3 time series	VV_{asc}, VH_{asc}, VV/VH_{asc}
			5 harmonic coefficients for each time series	a_1, a_2, b_1, b_2, c (Equation (4))
			7 median features for each time series	P_1, P_2, P_3, P_4, S_1, S_2, S_3
		S1 descending orbit	3 time series	VV_{des}, VH_{des}, VV/VH_{des}
			5 harmonic coefficients for each time series	a_1, a_2, b_1, b_2, c (Equation (4))
			7 median features for each time series	P_1, P_2, P_3, P_4, S_1, S_2, S_3
		S1 both orbits	9 time series	VV_{asc}, VH_{asc}, VV/VH_{asc}, VV_{des}, VH_{des}, VV/VH_{des}, VV_{asc}-VV_{des}, VH_{asc}-VH_{des}, VV/VH_{asc}-VV/VH_{des}
			5 harmonic coefficients for each time series	a_1, a_2, b_1, b_2, c (Equation (4))
			7 median features for each time series	P_1, P_2, P_3, P_4, S_1, S_2, S_3
	S1 polarimetric parameters	S1 ascending orbit	5 time series	$g0_{asc}$, $g1_{asc}$, Sh_{asc}, Sh_I_{asc}, Sh_P_{asc}
			5 harmonic coefficients for each time series	a_1, a_2, b_1, b_2, c (Equation (4))
			7 median features for each time series	P_1, P_2, P_3, P_4, S_1, S_2, S_3
		S1 descending orbit	5 time series	$g0_{des}$, $g1_{des}$, Sh_{des}, Sh_I_{des}, Sh_P_{dec}
			5 harmonic coefficients for each time series	a_1, a_2, b_1, b_2, c (Equation (4))
			7 median features for each time series	P_1, P_2, P_3, P_4, S_1, S_2, S_3
		S1 both orbits	15 time series	$g0_{asc}$, $g1_{asc}$, Sh_{asc}, Sh_I_{asc}, Sh_P_{asc}, $g0_{des}$, $g1_{des}$, Sh_{des}, Sh_I_{des}, Sh_P_{dec}, $g0_{asc}$-$g0_{des}$, $g1_{asc}$-$g1_{des}$, Sh_{asc}- Sh_{des}, Sh_I_{asc}- Sh_I_{des}, Sh_P_{asc}-Sh_P_{dec}
			5 harmonic coefficients for each time series	a_1, a_2, b_1, b_2, c (Equation (4))
			7 median features for each time series	P_1, P_2, P_3, P_4, S_1, S_2, S_3

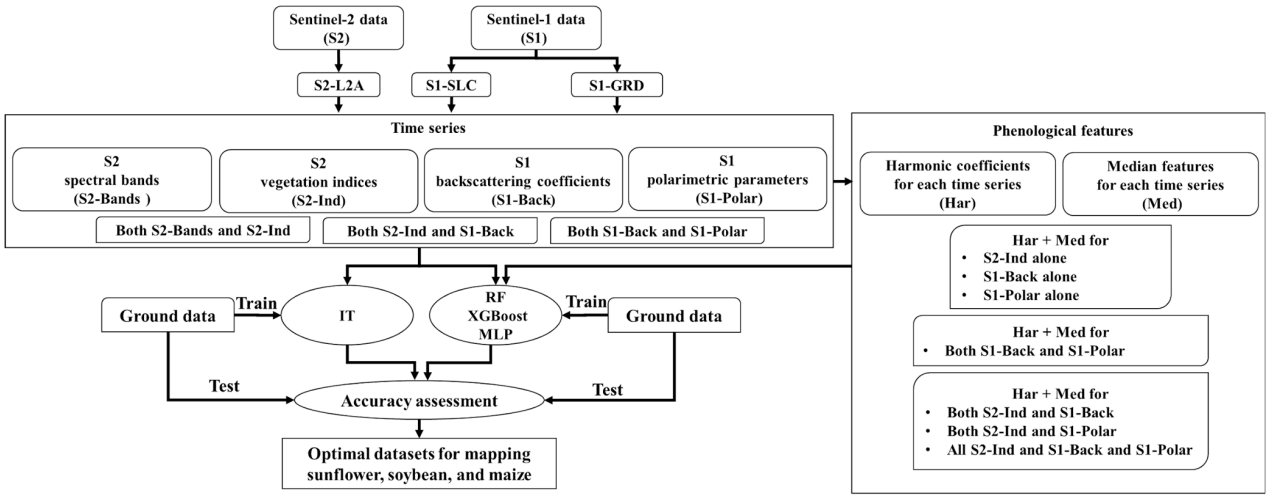

Figure 2. The flowchart of this study.

Harmonic Coefficients

We applied the Fourier transform, also known as harmonic regression, to model and capture variations in the satellite time series data for each field. This technique effectively characterizes changes in phenology across different crops such as sunflower, maize, and soybean [28,57,58]. Harmonic regression breaks down a time series into a series of simple cosine waves, along with an added constant term [59]. Harmonic regression allows us to capture the unique temporal patterns of each crop, enhancing our ability to differentiate between species based on their phenological behaviors. This approach aligns with our study's objective to accurately map crop types by leveraging these seasonal variations. Each time series of our datasets (Sections 2.2.2 and 2.2.3) is modeled as a time-dependent function f(t) with a harmonic regression expressed as:

$$f(t) = c + \sum_{k=1}^{n} [a_k \cos(2\pi\omega kt) + b_k \sin(2\pi\omega kt)] \quad (4)$$

where a_k and b_k represent, respectively, the cosine and sine coefficients, c is the intercept term, n is the harmonic regression order, and ω defines the function's period. The variable t corresponds to the day of the year that an image was taken, scaled between 0 (1 April) and 1 (1 December). To select the best regression, we tested different ω values and compared the R2 between the fitted function and the time series. So, we used a second-order harmonic regression (n = 2) with ω = 0.8. The application of this regression yielded a total of five features for each field and each S1 and S2 time series.

Monthly and Seasonal Medians

We used the methodology outlined by Qadir et al. [12] to compute monthly and seasonal medians for each field, considering both our S1 and S2 time series (Table 4). For each field and time series, we determined the median of all values during the four critical months of the phenological cycle for our selected summer crops (June, July, August and September). Additionally, three seasonal medians were calculated based on crop growth stages in our study sites: 1 April to 1 June, 1 June to 1 September, and 1 September to 1 December. As a result, we derived seven features from each S1 and S2 time series for each field based on these median calculations (hereafter referred to as median features). These features act as statistical representations of the satellite image time series throughout key periods of crop growth, effectively capturing the seasonal dynamics of crop development [38]. By focusing on monthly and seasonal medians, we capture the essential statistical characteristics of crop development throughout key growth stages, offering a robust summary of the time series that enhances the model's ability to differentiate crops based on seasonal or monthly dynamics.

2.3.2. Classification Algorithms

Three machine learning classifiers, namely Random Forest (RF), Extreme Gradient Boosting (XGBoost), and Multi-Layer Perceptron (MLP), were applied for mapping our three summer crops by evaluating different input data scenarios among our S1 and S2 data. RF is a popular machine learning method, making it a strong reference point for comparing the accuracy of other models. XGBoost is a more advanced machine learning technique that has shown high accuracy for crop mapping in previous studies [60–62]. MLP is a basic type of neural network that represents a simple form of artificial neural networks (ANNs). Additionally, the InceptionTime neural network, a specialized algorithm for time series classification, was used to classify the S1 and S2 time series data. The InceptionTime classifier is underexplored but has demonstrated high performance in previous studies on crop type mapping [63,64]. In our previous research, InceptionTime consistently outperformed other models, including RF, MLP, and LSTM_FCN, particularly in transfer scenarios [64]. It achieved the highest accuracy for crop mapping tasks and demonstrated remarkable stability, with the smallest range between minimum and maximum accuracy metrics. However, InceptionTime requires significantly more computation

time for the training stage compared to the other three classifiers. Employing these four algorithms enables us to evaluate the performance of a time series-specific algorithm that relies solely on non-tabular data (sequential data, such as time series) against general machine learning algorithms that utilize both tabular (structured data organized in rows and columns) and non-tabular data. In many cases, tune model hyperparameters can improve performance. However, in this study on model transferability, where the training and test datasets exhibit different distributions, optimizing hyperparameters based on a validation set that includes only held-out training data may not lead to robust results on the test set. For this reason, we chose to use default parameter settings, which are typically designed to perform adequately across a variety of general scenarios. The classification was conducted using Python 3.11. Our Python implementation codes for classification can be found at https://github.com/cassiofragadantas/Colza_Classif, accessed on 30 April 2024 and https://github.com/Saeideh-Maleki, accessed on 30 April 2024.

Random Forest (RF)

RF algorithm is an ensemble learning method that consists of multiple decision trees, where the output from each tree is aggregated to form the final prediction. Each decision tree operates on a different subset of the dataset, allowing RF to reduce variance and improve accuracy while mitigating overfitting tendencies. As a meta-estimator, RF builds these decision trees on various parts of the dataset and combines their outputs through majority voting for classification [65]. In this study, the number of trees was set to 100, and all other parameters were kept at their default values.

Multi-Layer Perceptron (MLP)

MLP is a deep learning model with a fully connected neural network architecture. In an MLP, neurons in one layer are connected to all neurons in the neighboring layers, forming a dense structure that allows the network to learn complex patterns in the data [66]. The MLP consists of multiple layers of nodes (neurons), each with associated weights and biases that are learned through backpropagation to minimize the difference between predicted and actual outcomes [30]. In this study, the MLP architecture used contained two hidden layers, each with 256 neurons, followed by batch normalization and a rectified linear unit (ReLU) activation function. To prevent overfitting, a dropout rate of 0.5 was applied during training.

Extreme Gradient Boosting (XGBoost)

XGBoost is an advanced machine learning algorithm that builds on the principles of gradient boosting to create highly accurate and efficient models. Unlike traditional gradient boosting, XGBoost incorporates various optimizations, such as regularization to prevent overfitting, parallel processing, and handling of missing data, making it well-suited for large-scale datasets [67]. XGBoost sequentially builds decision trees, where each subsequent tree attempts to correct the errors of the previous trees by focusing on the misclassified samples [68]. The algorithm minimizes a loss function through gradient descent, adjusting the weights of the trees iteratively to improve accuracy. In this study, the hyperparameters for XGBoost were set to their default values.

InceptionTime

IT, introduced by Fawaz et al. [69], is designed for multivariate time series analysis. It consists of an ensemble of five deep learning models, each containing two residual blocks, which in turn are composed of inception modules. These inception modules apply one-dimensional convolutional filters of varying lengths to the input time series data, allowing the model to capture patterns at multiple scales simultaneously. A key feature of InceptionTime is the use of shortcut connections between residual blocks, which mitigate the vanishing gradient problem often encountered in deep networks. By leveraging this architecture, InceptionTime achieves high accuracy in time series classification, while

reducing the risk of overfitting through its ensemble approach. As the default hyperparameters generally perform well, this study maintained the default configuration during deployment [69].

2.3.3. Summer Crop Types Mapping

To evaluate the potential of S1 and S2 images and their extracted features in mapping three summer crops—maize, sunflower, and soybean—we employed RF, MLP, and XGBoost to classify our datasets across several dataset scenarios and train-test combinations. The classification categories included four classes: maize, sunflower, soybean, and other crops.

Classification was performed using one of the following dataset scenarios (only the main tested configurations are listed):

S2 images

- Spectral bands time series
- Vegetation indices time series
- Both spectral bands and vegetation indices
- Harmonic coefficients extracted from S2 vegetation indices
- Median features extracted from S2 vegetation indices
- Both harmonic coefficients and median features from S2 vegetation indices

S1 images

For S1 data, we also assessed the impact of orbit type by testing the following scenarios with separate ascending and descending orbits, as well as their combination:

Backscattering coefficients

- S1 backscattering coefficients time series (separate orbits and combined orbits)
- Harmonic coefficients extracted from S1 backscattering coefficients time series (separate orbits and combined orbits)
- Median features extracted from S1 backscattering coefficients time series (separate orbits and combined orbits)
- Both harmonic coefficients and median features from S1 backscattering coefficients time series (combined orbits)

Polarimetric parameters

- S1 polarimetric parameters time series (separate orbits and combined orbits)
- Harmonic coefficients extracted from S1 polarimetric parameters time series (separate orbits and combined orbits)
- Median features extracted from S1 polarimetric parameters time series (separate orbits and combined orbits)
- Both harmonic coefficients and median features from S1 polarimetric parameters time series (combined orbits)
- A combined dataset of S1 backscattering coefficients and polarimetric parameters time series

S1 and S2 images

- S1 backscattering coefficients and S2 vegetation indices time series
- Harmonic coefficients and median features extracted from S1 backscattering coefficients and S2 vegetation indices
- Harmonic coefficients and median features extracted from S1 polarimetric parameters and S2 vegetation indices
- Harmonic coefficients and median features extracted from S1 backscattering coefficients, S1 polarimetric parameters, and S2 vegetation indices

In addition to scenarios used for RF, XGBoost, and MLP classifiers, some scenarios were tested for the InceptionTime classifier in order to classify the S2 and S1 time series. This approach allowed us to compare the performance of a time series-specific algorithm, which processes sequential data, with general machine learning algorithms that process both

structured (tabular) and sequential (non-tabular) data (RF, XGBoost, MLP). The datasets classified by InceptionTime included:

- S2 vegetation indices time series
- S1 backscattering coefficients time series (separate orbits, and combined orbits)
- S1 polarimetric parameters time series (separate orbits and combined orbits)
- A combined dataset of S1 backscattering coefficients and S2 vegetation indices time series
- A combined dataset of S1 backscattering coefficients and polarimetric parameters time series

For each dataset scenario, different configurations of study sites and years were used for training and testing (Table 5). These configurations enable to analyze the spatial transferability, the temporal transferability, and the spatiotemporal transferability of tested classifiers:

- Spatial transferability: Different study sites were used for training and testing within the same year (e.g., Tarbes 2020 for training and Dijon 2020 for testing, or Dijon 2020 for training and Tarbes 2020 for testing).
- Temporal transferability: The same study site was used for training and testing, but across different years (e.g., Tarbes 2020 for training and Tarbes 2021 for testing, or Tarbes 2021 for training and Tarbes 2020 for testing).
- Spatiotemporal transferability: Different study sites and years were used for training and testing (e.g., Tarbes 2021 for training and Dijon 2020 for testing, or Dijon 2020 for training and Tarbes 2021 for testing).

Table 5. Summary of transferability scenarios for spatial, temporal, and spatiotemporal analyses, along with the number of agricultural plots used in each dataset.

Transfer Scenario	Train Site/Year	Test Site/Year	Number of Agricultural Plots in Train Dataset	Number of Agricultural Plots in Test Dataset
Spatial transferability	Tarbes 2020	Dijon 2020	76,153	43,670
	Dijon 2020	Tarbes 2020	43,670	76,153
Temporal transferability	Tarbes 2020	Tarbes 2021	76,153	93,654
	Tarbes 2021	Tarbes 2020	93,654	76,153
Spatiotemporal transferability	Tarbes 2021	Dijon 2020	93,654	43,670
	Dijon 2020	Tarbes 2021	43,670	93,654

2.4. Evaluation Metrics

To assess the performance of the classification approaches, we first evaluated the F1-score per class across all scenarios to identify the best-performing results. Once the best scenarios were selected, we further analyzed them using Precision, Recall, and F1-Score (per class). It should be noted that in this article, primarily the F1-Scores will be provided. The equations for the accuracy metrics are provided in Appendix A.

3. Results

3.1. Trends in S2 Vegetation Indices and S1 Data for Three Summer Crops Mapping

3.1.1. RENDVI and NDVI Trends for Sunflower, Soybean, and Maize

The temporal dynamics of RENVDI and NDVI for our three summer crops—sunflower, soybean, and maize—in Tarbes 2021 are presented in Figure 3a,b. The RENDVI and NDVI were chosen as two examples to highlight the trends in the S2 vegetation indices for the three crops because these indices appeared to be the two most important indices according to the RF feature importance analysis. Additional details on the RF feature importance can be found in the Appendix B (Figure A1).

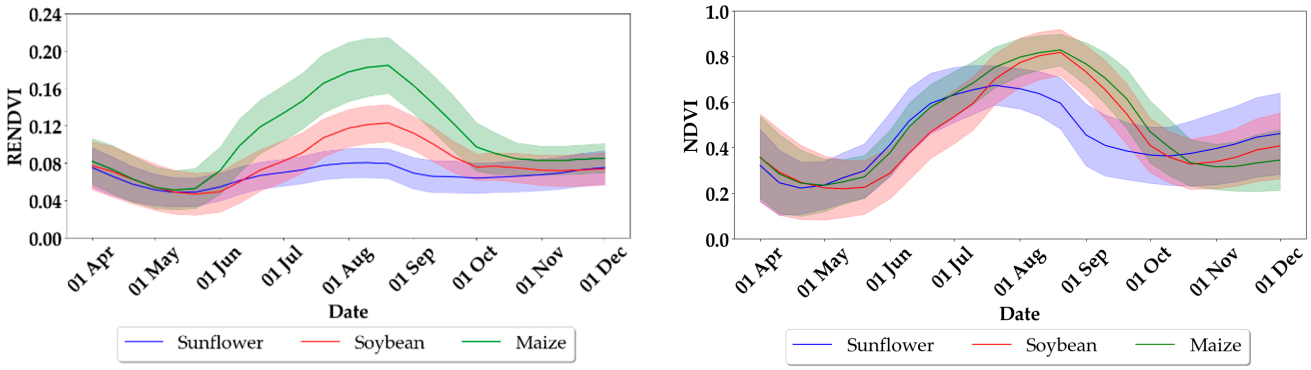

(**a**) (**b**)

Figure 3. Temporal behavior of RENVDI (**a**) and NDVI (**b**) for sunflower, soybean, and maize in Tarbes 2021. The graphs display the mean values of all fields for each crop, while the shaded areas represent the standard deviation.

RENVDI and NDVI show a gradual increase for all three crops starting in May, which corresponds to the emergence stage. As the plants grow, both indices rise. RENVDI peaks in August for sunflower, soybean, and maize, with peak values of 0.08 for sunflower, 0.12 for soybean, and 0.18 for maize. For NDVI, sunflower reaches a peak of 0.7 in mid-July, whereas soybean and maize peak at 0.9 in mid-August. After reaching their peaks, both indices decline for all three crops, continuing until the beginning of September for sunflower and until October for soybean and maize. The decline in RENVDI from the peak is 0.02 for sunflower, 0.04 for soybean, and 0.08 for maize. For NDVI, the decline from the peak is 0.2 for sunflower and 0.4 for soybean and maize, indicating the end of the growth period. The shorter growth period of sunflower and the differences in RENVDI levels among the three crops serve as valuable indicators for mapping sunflower, soybean, and maize.

3.1.2. S1 Backscattering and Polarimetric Trends for Sunflower, Soybean, and Maize

Figure 4 presents the temporal variation in the top four important S1 backscattering coefficients channels for mapping sunflower, soybean, and maize in Tarbes 2021, ranked by RF feature importance (Appendix B, Figure A2a).

The variability in both VV and VH polarizations is seen just after sowing (April–May) due to the interaction of the microwave signal with the bare soil before this period (radar signal increases as soil moisture increases). From May onwards, due to the development of vegetation, VV and VH increase sharply. In VV, this increase is significant for sunflower, with the signal increasing from −12 dB in May to around −6 dB in July. The increase is smaller between May and July for soybean and maize, with the VV signal rising from −12 dB to −8 dB for soybean and from −12 dB to −10 dB for maize. VV then begins to decrease sharply from August for sunflower and from September for soybean and maize (vegetation drying out). For VH, a similar pattern is observed for summer crops, with a sharp increase between April/May and July/August, followed by a decrease from early October. Analysis of VV and VH shows better discrimination potential with VV than with VH, as shown by the variable importance analysis (Appendix B, Figure A2a).

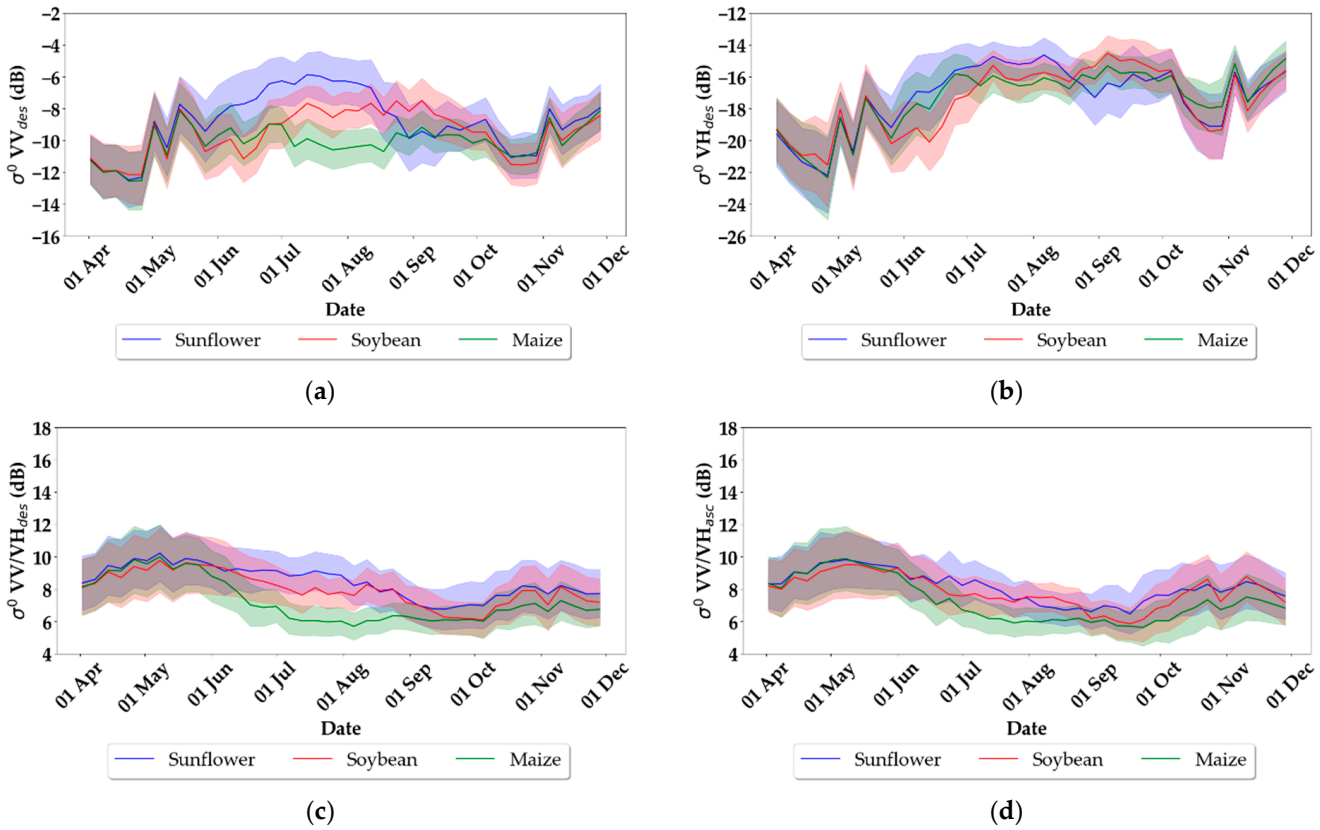

Figure 4. Temporal variation in the most important S1 backscattering coefficients channels (ranked by RF feature importance) for sunflower, soybean, and maize in Tarbes 2021: (**a**) VV_{des}, (**b**) VH_{des}, (**c**) VV/VH_{des} (the most significant), (**d**) VV/VH_{asc}. The graphs display the mean values of all fields for each crop, while the shaded areas represent the standard deviation.

The VV/VH ratio for both descending and ascending orbits decreases as the vegetation grows. In the descending orbit, maize shows the sharpest drop, decreasing from 10 dB in May to 6 dB from July onwards, remaining approximately stable until October. Soybean's ratio decreases from 10 dB in May to 8 dB by mid-July, remaining constant until late August, before further dropping to 6 dB in September. Sunflower shows a steady decline from 10 dB in May to 7 dB by September. A similar behavior is observed in the ascending orbit, though the trends are more pronounced in the descending orbit, with greater differentiation between the three crops.

Figure 5 presents the temporal behavior of the six most important S1 polarimetric parameters across both orbits for sunflower, soybean, and maize in Tarbes 2021, based on RF feature importance (details in the Appendix B, Figure A2b). The two most significant parameters are Shannon_P for both ascending and descending orbits. Shannon_P increases with the vegetation development for all three crops, but at different rates for each crop. Maize shows the highest rate of change over a shorter period, with values increasing from −0.75 in May to −0.4 in early July. Soybean values increase more gradually, from −0.75 in May to −0.4 in the beginning of October. Sunflower shows a very slow increase over time, from −0.75 in May to just −0.7 in early August, then peaking at −0.45 in mid-September. The remaining four polarimetric parameters ($g1_{asc}$, $Shannon_{asc}$, $Shannon\_I_{asc}$, $g0_{asc}$) show similar patterns to those observed for the VV and VH polarizations.

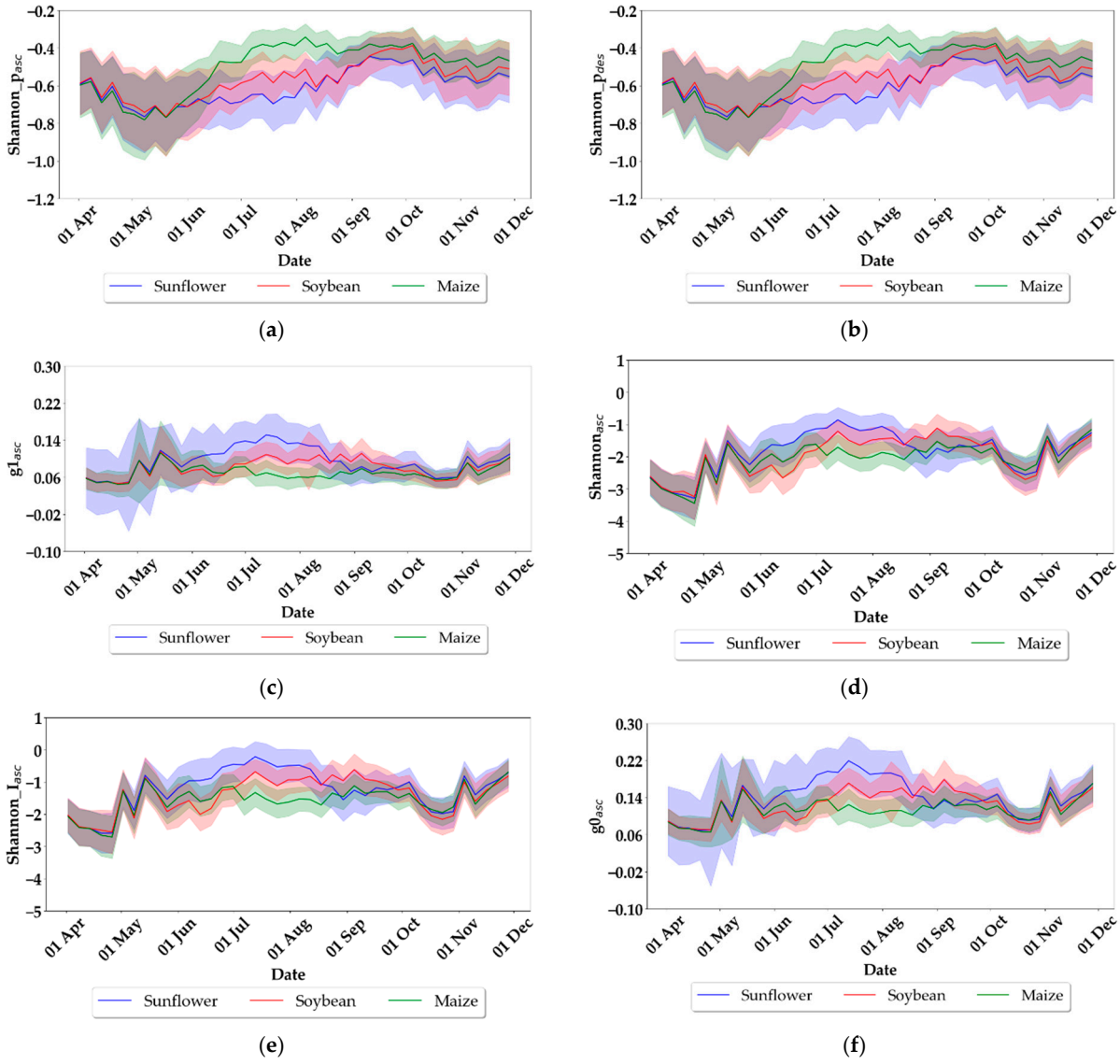

Figure 5. Temporal variation in the most important S1 polarimetric parameters (ranked by RF feature importance) in Tarbes 2021: (**a**) Shannon_P$_{asc}$, (**b**) Shannon_P$_{des}$, (**c**) g1$_{asc}$, (**d**) Shannon$_{asc}$, (**e**) Shannon_I$_{asc}$, (**f**) g0asc. The graphs display the mean values of all fields for each crop, while the shaded areas represent the standard deviation.

3.2. Summer Crops Mapping

3.2.1. Using S2 Images

We evaluated three algorithms—RF, XGBoost, and MLP—for mapping sunflower, soybean, and maize using S2 images. On one hand, we used time series of spectral bands, vegetation indices, and their combination; on the other hand, we utilized phenological features (harmonic coefficients and median features) derived from each S2 time series. Figure 6 illustrates the best results obtained from the S2 datasets, all of which were related to vegetation indices. Among the three classifiers, XGBoost and MLP produced similar F1 scores, both outperforming RF. Specifically, when using vegetation indices time series with the XGBoost classifier, the average F1 scores across six combinations of study sites and years were 75.4% for sunflower, 67.9% for soybean, and 90.1% for maize. MLP achieved F1 scores of 74.9% for sunflower, 71.1% for soybean, and 89.4% for maize. In contrast, RF's F1 scores were 69.5% for sunflower, 60.5% for soybean, and 88.0% for maize. When using S2 spectral bands, the mean F1 scores across all six combinations of study sites and years were approximately 5% lower than those derived from S2 vegetation indices. The

combination of S2 indices and spectral bands produced F1 scores comparable to those obtained from vegetation indices alone. Specifically, when using the combined vegetation indices and spectral bands, XGBoost achieved mean F1 scores of 76.3% for sunflower, 68.4% for soybean, and 90.1% for maize across the six combinations of study sites and years.

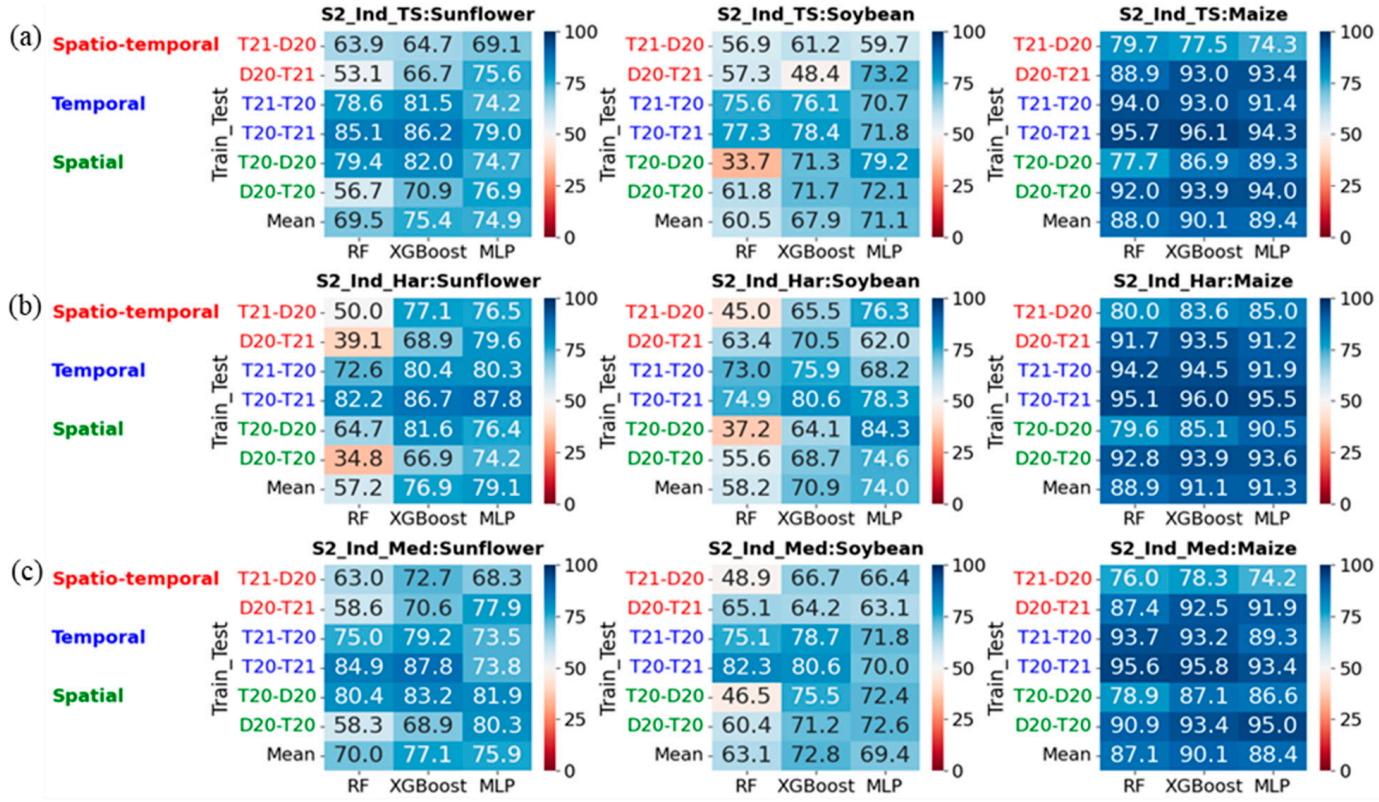

Figure 6. F1 scores obtained using (**a**) S2 vegetation indices time series, (**b**) harmonic coefficients, and (**c**) median features with RF, XGBoost, and MLP classifiers across six combinations of study sites and years as train and test. Ind = vegetation indices, TS = time series, Har = harmonic coefficients, Med = median features. T21 = Tarbes 2021, T20 = Tarbes 2020, D20 = Dijon 2020.

As shown in Figure 6, median features derived from S2 vegetation indices produced similar F1 scores to harmonic coefficients, particularly for XGBoost and MLP. For the harmonic coefficients extracted from the S2 vegetation indices time series, XGBoost and MLP again outperformed RF. The average F1 score for XGBoost was 76.9% for sunflower, 70.9% for soybean, and 91.1% for maize. MLP achieved mean F1 scores of 79.1% for sunflower, 74.0% for soybean, and 91.3% for maize. In contrast, RF had lower mean F1 scores: 57.2% for sunflower, 58.2% for soybean, and 88.9% for maize. Classification results using median features extracted from vegetation indices time series revealed similar performance to that of harmonic features. XGBoost and MLP performed similarly, with XGBoost achieving an average F1 score of 77.1% for sunflower, 72.8% for soybean, and 90.1% for maize. MLP's mean F1 scores were 75.9% for sunflower, 69.4% for soybean, and 88.4% for maize, while RF achieved scores of 70.0% for sunflower, 63.1% for soybean, and 87.1% for maize. The combination of both harmonic and median features derived from S2 vegetation indices yielded results similar to those from median features alone.

3.2.2. Using S1 Images

We evaluated the potential of S1 images to map maize, sunflower, and soybean using different sets of input data: time series data (backscattering coefficients and polarimetric parameters) and features calculated using these time series, including harmonic coefficients and median features. Figures 7–12 show the results obtained with backscattering coeffi-

cients and polarimetric data, respectively. In each case, we assessed the impact of S1 orbit type (ascending, descending).

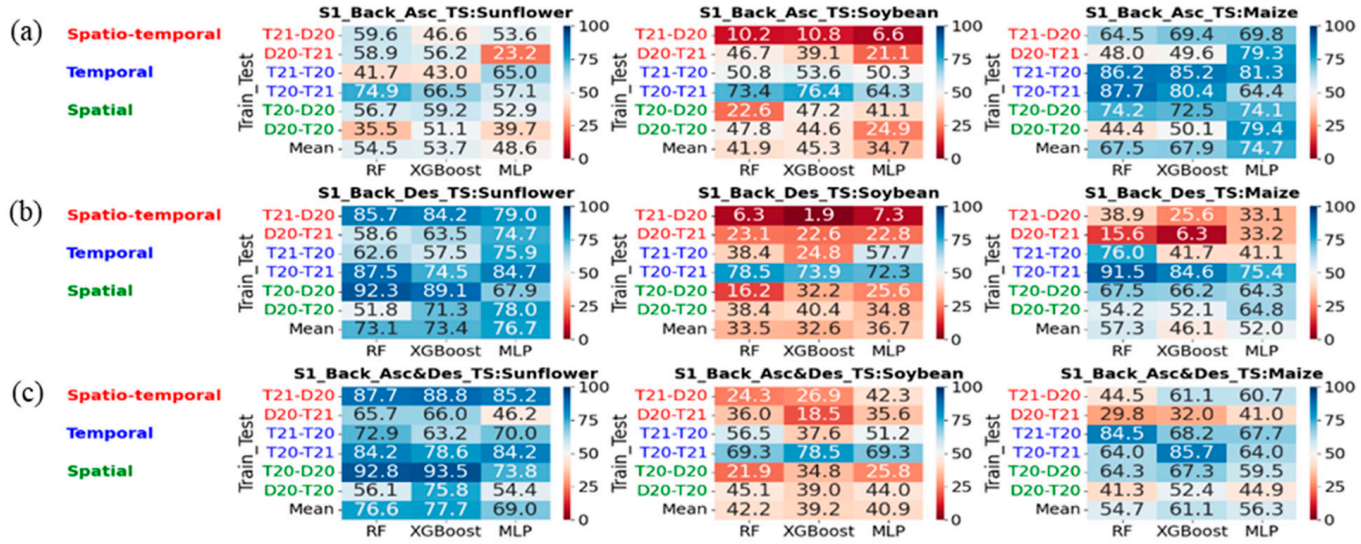

Figure 7. F1 scores obtained using S1 backscattering coefficients time series for (**a**) ascending orbit (Asc), (**b**) descending orbit (Des), and (**c**) their combination. These were evaluated with RF, XGBoost, and MLP classifiers across six train-test combinations of study sites and years. Key terms: Back = backscattering coefficients, TS = time series, T21 = Tarbes 2021, T20 = Tarbes 2020, D20 = Dijon 2020.

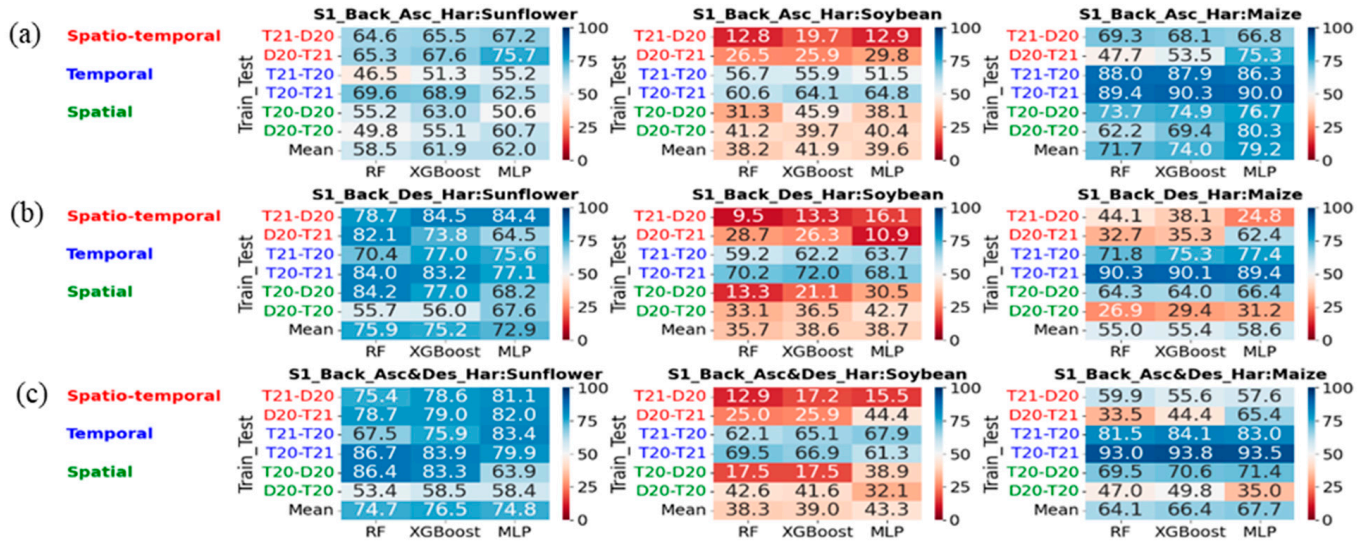

Figure 8. F1 scores were obtained using harmonic coefficients derived from S1 backscattering time series for (**a**) ascending orbit (Asc), (**b**) descending orbit (Des), and (**c**) their combination. These were evaluated with RF, XGBoost, and MLP classifiers across six train-test combinations of study sites and years. Key terms: Back = backscattering coefficients, Har = harmonic coefficients, T21 = Tarbes 2021, T20 = Tarbes 2020, D20 = Dijon 2020.

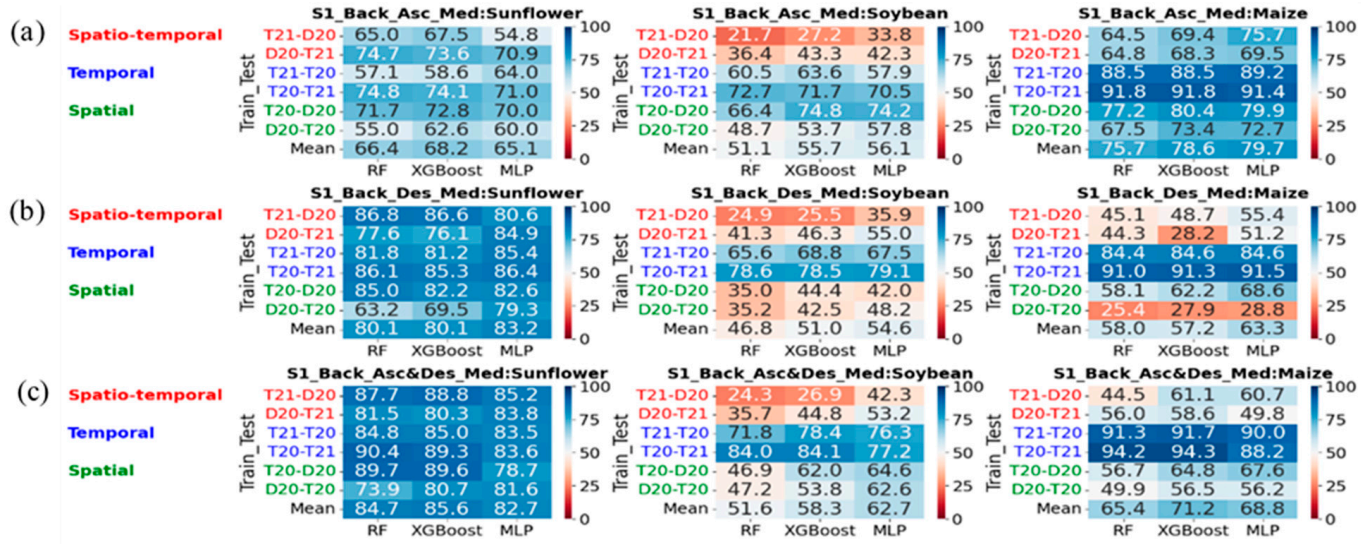

Figure 9. F1 scores were obtained using median features derived from S1 backscattering time series for (**a**) ascending orbit (Asc), (**b**) descending orbit (Des), and (**c**) their combination. These were evaluated with RF, XGBoost, and MLP classifiers across six train-test combinations of study sites and years. Key terms: Back = backscattering coefficients, Med = median features, T21 = Tarbes 2021, T20 = Tarbes 2020, D20 = Dijon 2020.

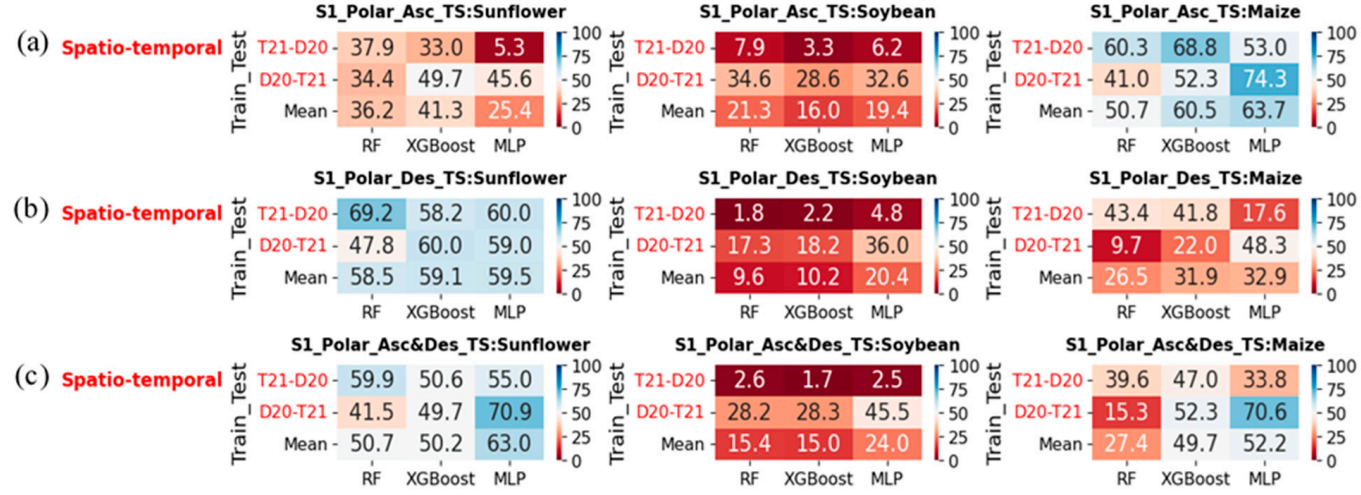

Figure 10. F1 scores obtained using S1 polarimetric parameters time series for (**a**) ascending orbit (Asc), (**b**) descending orbit (Des), and (**c**) their combination. These were evaluated with RF, XGBoost, and MLP classifiers across six train-test combinations of study sites and years. Key terms: Polar = Polarimetric parameters, TS = time series, T21 = Tarbes 2021, D20 = Dijon 2020.

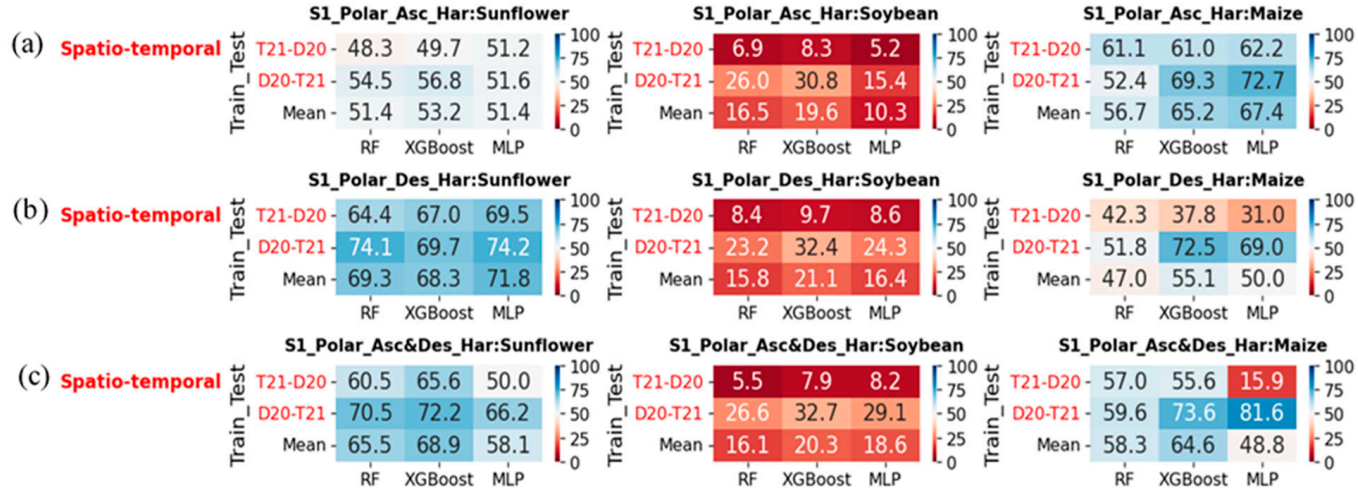

Figure 11. F1 scores were obtained using harmonic coefficients derived from S1 polarimetric parameters time series for (**a**) ascending orbit (Asc), (**b**) descending orbit (Des), and (**c**) their combination. These were evaluated with RF, XGBoost, and MLP classifiers across six train-test combinations of study sites and years. Key terms: Polar = Polarimetric parameters, Har = harmonic coefficients, T21 = Tarbes 2021, D20 = Dijon 2020.

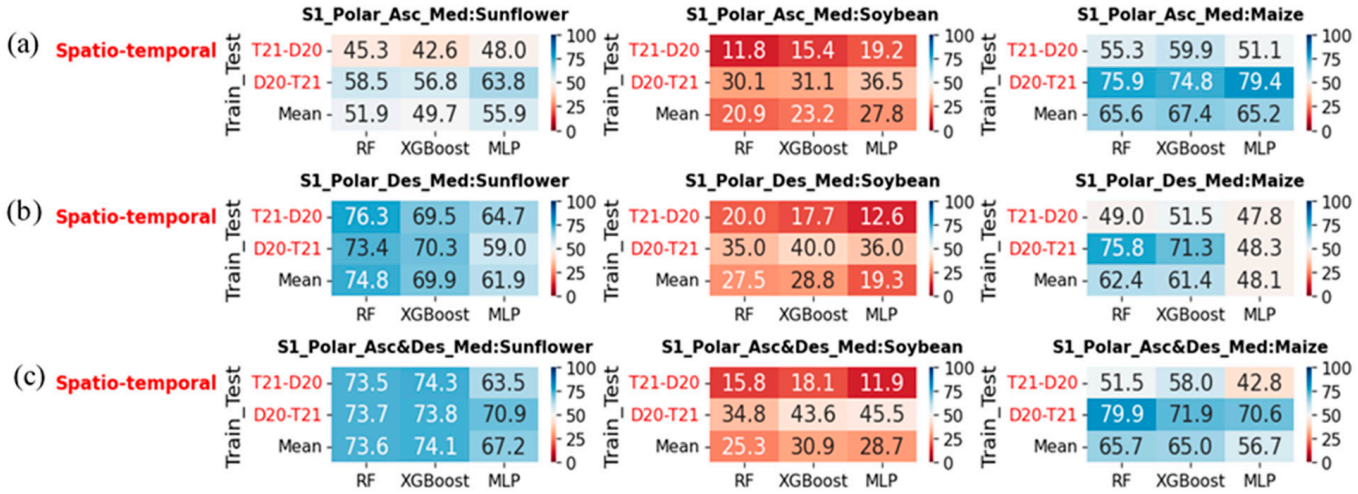

Figure 12. F1 scores were obtained using median features derived from S1 polarimetric parameters time series for (**a**) ascending orbit (Asc), (**b**) descending orbit (Des), and (**c**) their combination. These were evaluated with RF, XGBoost, and MLP classifiers across six train-test combinations of study sites and years. Key terms: Polar = Polarimetric parameters, Med = median features, T21 = Tarbes 2021, D20 = Dijon 2020.

Using Backscattering Coefficients

Using the S1 backscattering coefficients time series for sunflower mapping, the best results were obtained either with the descending orbit alone or with both ascending and descending orbits together (Figure 7). Among the three classifiers tested, XGBoost appeared slightly better, though its performance was quite close to RF and MLP. Results with the ascending orbit were about 20% lower than the descending orbit. For example, the XGBoost classifier achieved an average F1 score of 77.7% for sunflower with both orbits combined, 73.4% with the descending orbit, and 53.7% with the ascending orbit. Figure 7 also shows that F1 scores for soybean mapping are relatively low across all S1 orbit configurations and classifiers, with the highest mean F1 score being 45.3% using XGBoost and the ascending orbit. For maize, the best result was obtained with the ascending orbit and MLP classifier

(74.7%), although XGBoost and RF also provided good results (67.9% with XGBoost and 67.5% with RF). The lowest performance for maize was obtained with the descending orbit. The best classification of the three summer crops using backscattering coefficients was achieved with XGBoost and the combination of ascending and descending orbits, yielding F1 scores of 77.7% for sunflower, 39.2% for soybean, and 61.1% for maize.

The use of the harmonic coefficients did not improve the mapping of the three summer crops compared to the use of the backscattering coefficients time series (Figure 8). While the performance of the three classifiers was different using backscattering coefficients time series, the performance of our three classifiers was similar when using harmonic coefficients. The optimal dataset for mapping the three summer crops was the combination of ascending and descending orbits with the XGBoost classifier, achieving an F1 score of 76.5% for sunflower, 39.0% for soybean, and 66.4% for maize. However, focusing on each crop, sunflower mapping performs the best with descending alone or with ascending and descending together, soybean mapping does not vary across orbit configurations, and maize mapping achieves the best results with the ascending orbit.

Using median features for classifying summer crops yielded better results than S1 backscattering coefficients time series (Figure 9). For sunflower, the best accuracy was achieved with either the descending orbit alone or the combination of ascending and descending orbits, with the highest mean F1 score of 85.6% using XGBoost. Soybean mapping showed lower accuracy across all orbit configurations, with the highest F1 scores for the combination of ascending and descending orbits using MLP (62.7%) or XGBoost (58.3%). Maize was best classified with the ascending orbit, followed by the combined orbits, with all three classifiers performing similarly (75.7% for RF, 78.6% for XGBoost, and 79.7% for MLP). Therefore, for effective mapping of all three summer crops using median features, the best configuration is the combination of both orbits with XGBoost, achieving F1 scores of 85.6% for sunflower, 58.3% for soybean, and 71.2% for maize.

Compared to the best results obtained with S1 backscattering coefficients, the use of median features with XGBoost provided higher F1 scores. For sunflower, median features of S1 backscattering improved the F1 score by approximately 8% compared to using backscattering coefficients time series alone. For soybean, the improvement was about 19%, and for maize, it was around 11%.

Using Polarimetric Parameters

Figure 10 presents the classification results using S1 polarimetric time series for sunflower, soybean, and maize. Due to the high computational time required for the generation of polarimetric parameters, we calculated these parameters only for a spatio-temporal transfer scenario. The results indicate that the S1 polarimetric time series were less effective compared to the backscattering coefficients time series. Among the polarimetric time series of ascending, descending and their combination, the maximum F1 score for sunflower was around 63.0% using both orbits and MLP. For soybean, the results were low, with a maximum F1 score of 24.0% using both orbits and MLP. Maize classification achieved a maximum F1 score of 63.7% with MLP and 60.5% with XGBoost in the ascending orbit.

Using harmonic coefficients derived from the time series of polarimetric parameters (Figure 11), the classification performance improved compared to the polarimetric time series results. The best F1 scores for sunflower were obtained from descending orbit alone or from both orbits (68.3% for XGBoost, 69.2% for RF, and 71.8% for MLP). Soybean classification accuracy remained low, with a maximum of 21.1% using XGBoost in the descending orbit. For maize, the best mean F1 score using harmonic coefficients was 67.4% using MLP and the ascending orbit.

Within the median features derived from each orbit configurations of polarimetric time series, the combination of both orbits showed the best classification for sunflower with a mean F1 score of almost 74.0% for RF and XGBoost and 67.2% for MLP (Figure 12). The mean F1 score for soybean reached 30.9% using XGBoost and both orbits, which seemed ineffective for classification. For maize, the best results within the median features were again obtained from the ascending orbit, with mean F1 score between 65.0% and 67.0% for all three algorithms. The combination of medians and harmonic coefficients did not improve the F1 scores for any crop across all algorithms.

When comparing the results using polarimetric parameters (time series, harmonic coefficients, median features), the median results were higher but still significantly lower than those obtained with median features calculated from the backscattering coefficients.

Using S1 Backscattering Coefficients and Polarimetric Parameters

Combining time series of backscattering coefficients and polarimetric parameters did not yield better results for classifying the three summer crops. The accuracy obtained was lower than that achieved with the backscattering coefficients time series alone. Similarly, the combination of harmonic coefficients and median features did not provide better classification.

3.2.3. Using S1 and S2 Images

We evaluated four combinations using S1 and S2 data, including time series of S2 vegetation indices and S1 backscattering coefficients, harmonic coefficients and median features calculated from the S2 vegetation indices and S1 backscattering coefficients time series, harmonic coefficients and median features of S2 vegetation indices and S1 polarimetric parameters, and finally a combination of harmonic coefficients and median features of S2 vegetation indices, S1 backscattering coefficients, and S1 polarimetric parameters. Figure 13 shows the classification results for these scenarios. The best results were obtained using the combination of harmonic coefficients and median features of S2 vegetation indices and S1 backscattering coefficients with XGBoost, which slightly outperformed RF and MLP (mean F1 scores: 89.9% for sunflower, 76.0% for soybean, and 91.1% for maize). This represents an improvement of 12.5% and 4% for sunflower and soybean, respectively, but the same value for maize classification compared to the use of the median or harmonic features extracted from S2 indices alone, which gave the best results among all S1 and S2 datasets separately. In addition, the combination of S2 indices and S1 backscattering coefficients time series performed well in all three classifiers with slightly better results using XGBoost, achieving mean F1 scores of 87.4% for sunflower, 72.0% for soybean, and 89.7% for maize.

3.2.4. Using Time Series Dataset with the IT Classifier

In addition to the previous evaluations of our three crops mapping using tabular and non-tabular data with RF, XGBoost, and MLP, we also tested the use of the InceptionTime classifier for time series classification (as detailed in Section 2.3.3). Our previous studies [63,64] demonstrated that the InceptionTime classifier achieved higher accuracy in crop mapping compared to RF and MLP classifiers. However, the InceptionTime classifier requires considerable computation time. For instance, using a standard machine with no graphics processing unit (GPU) (8 core CPU, 64 GB RAM), training on the S2 vegetation indices time series dataset for Tarbes 2021 (comprising 200,029 fields, 41 time steps, and 13 features) and classifying the S2 vegetation indices time series dataset for Dijon 2020 (comprising 96,815 fields, 41 time steps, and 13 features) took 35.57 h. In contrast, RF required 15 min, XGBoost 5 min, and MLP 20 min with the same datasets.

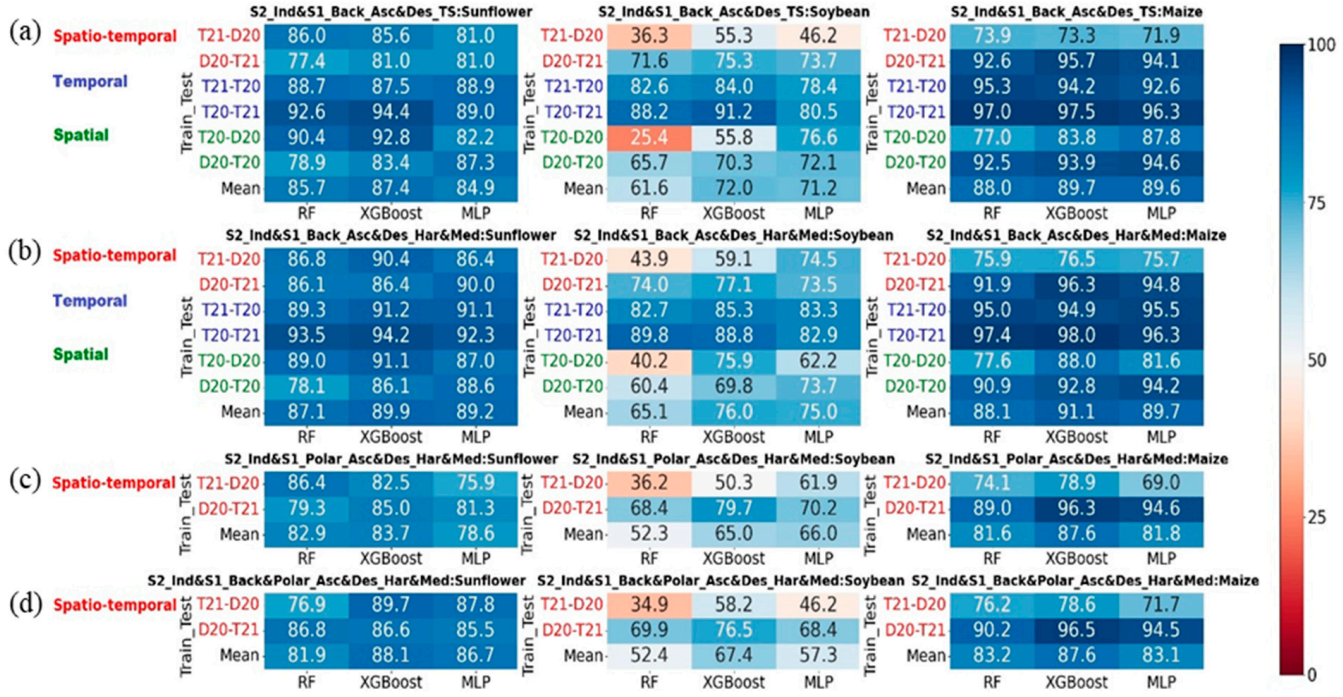

Figure 13. F1 scores obtained using various combinations of S1 and S2 data including: (**a**) time series of S2 vegetation indices and S1 backscattering coefficients, (**b**) harmonic coefficients and median features calculated from S2 vegetation indices and S1 backscattering coefficients, (**c**) harmonic coefficients and median features of S2 vegetation indices and S1 polarimetric parameters, and (**d**) a combination of harmonic coefficients and median features of S2 vegetation indices, S1 backscattering coefficients, and S1 polarimetric parameters. These combinations were evaluated using RF, XGBoost, and MLP classifiers across different combinations of study sites and years as train and test. Ind = vegetation indices, Back = backscattering coefficients, Polar = polarimetric parameters, TS = time series, Des = descending orbit, Asc = ascending orbit, Har = harmonic coefficients, Med = median features. T21 = Tarbes 2021, T20 = Tarbes 2020, D20 = Dijon 2020.

Figure 14 illustrates the performance of the InceptionTime classifier using the top three configurations tested with RF, XGBoost, and MLP including the S2 vegetation indices time series, S1 backscattering coefficients time series, and the combination of both S2 vegetation indices and S1 backscattering coefficients time series. Using the S2 vegetation indices time series, the InceptionTime classifier yielded F1 scores of 85.4% for mapping sunflower, 84.6% for soybean, and 93.1% for maize. The use of S1 backscattering coefficients from both orbits resulted in F1 scores of 87.2% for sunflower, 63.6% for soybean, and 81.7% for maize. Combining both S2 vegetation indices and S1 backscattering coefficients time series provided the best performance, with F1 scores close to 90% for all three crops (90.6% for sunflower, 86.1% for soybean, and 93.5% for maize). Conversely, using the InceptionTime classifier with S1 polarimetric parameters time series or with a combination of S1 backscattering coefficients and S1 polarimetric parameters time series resulted in lower accuracy compared to the three configurations mentioned above.

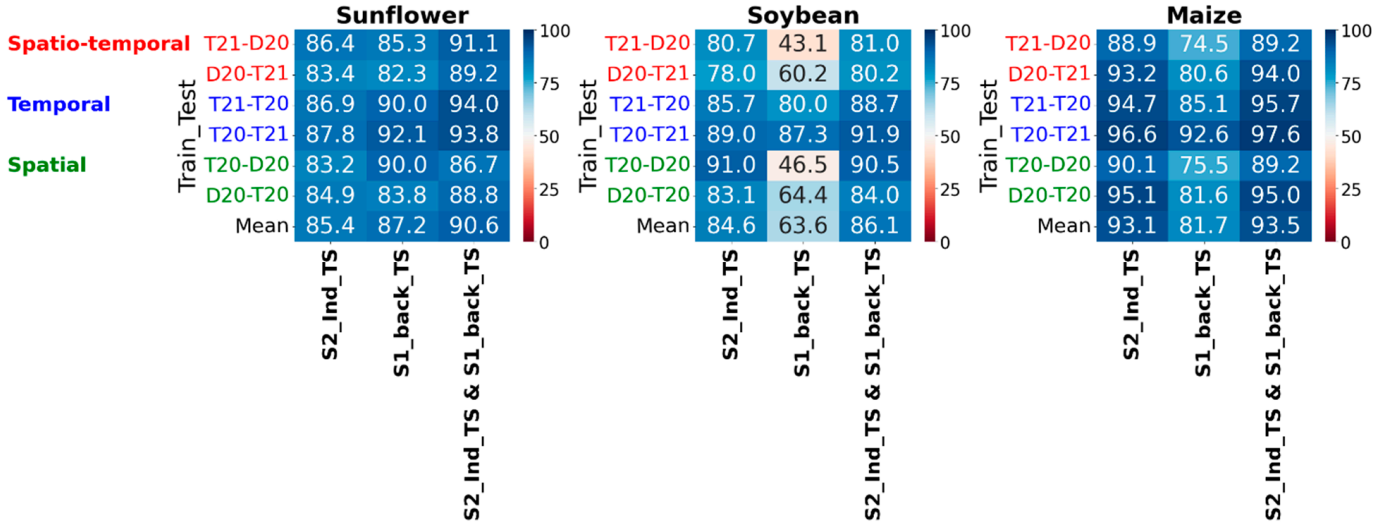

Figure 14. The performance of the InceptionTime classifier using the top three configurations tested with RF, XGBoost, and MLP: S2 vegetation indices time series, S1 backscattering coefficients time series, and the combination of both S2 vegetation indices and S1 backscattering coefficients time series. Ind = vegetation indices, TS = time series, Back = backscattering coefficients. T21 = Tarbes 2021, T20 = Tarbes 2020, D20 = Dijon 2020. The performances of the three configurations shown in this figure with InceptionTime are to be compared with the performances obtained with the other three classifiers (RF, XGBoost, and MLP) in Figure 6a, Figure 7c, and Figure 13a, respectively.

4. Discussion

4.1. Classification Performance Analysis

The classification experiments of sunflower, maize and soybean using RF, XGBoost, and MLP revealed that XGBoost consistently achieved the highest F1 scores across all cases, with MLP performing closely behind (Table 6). Conversely, RF exhibited the lowest performance. While both RF and XGBoost are decision tree-based algorithms [70], XGBoost outperformed RF due to its greater flexibility and ability to correct residual errors by generating new trees complementary to the previous ones, whereas RF's trees are generated independently from each other [71]. Previous studies have also shown that XGBoost demonstrates high performance in crop detection, even across large study sites [30,72–74], as it effectively captures complex nonlinear relationships in extensive datasets and delivers stable prediction results [47]. A literature review also revealed that XGBoost outperforms traditional classifiers such as SVM. For example, studies by Sun et al. [75], Prins and Niekerk [61], He et al. [62] found that XGBoost achieved higher accuracy than SVM. Furthermore, Saini and Ghosh [76] showed that XGBoost outperformed both RF and SVM when using spectral features. Given the superior performance of the XGBoost classifier over RF, and MLP, we now focus our discussion on the results of the XGBoost classifier.

To identify the most effective dataset for classifying sunflower, soybean, and maize, we compared the classification accuracy of three primary satellite data sources: optical images, radar backscattering, and polarimetric parameters. We evaluated both time series datasets (including S2 spectral bands, S2 vegetation indices, S1 backscattering coefficients, and polarimetric parameters) and extracted phenological features (harmonic coefficients and median features).

Our results showed that the highest mean F1 score across all algorithms for classifying the three crops was achieved using S2 vegetation indices, with close results between time series data and phenological features. Polarimetric data, however, produced the lowest results. Analysis of RF feature importance (details in the Appendix B, Figure A3) also highlighted the S2 vegetation indices as the most important features, as these indices capture detailed information about crop growth and health through multiple spectral bands that are sensitive to various plant developmental stages. The lower performance

of polarimetric parameters prompted an analysis of precision and recall for classifications based on median features from polarimetric data (the best-performing polarimetric dataset). Results showed both low precision and recall for soybean, along with low recall for maize and sunflower. For example, with the XGBoost classifier, precision for sunflower, soybean, and maize was 80.3%, 62.9%, and 82.6%, respectively, while recall was 60.2%, 25.1%, and 47.2%. The low precision for soybean suggests confusion with other crops, while the overall low recall across all three crops indicates many true instances were missed, limiting the reliability of comprehensive crop mapping. Additionally, we calculated the Jeffries–Matusita distance for separability analysis of S1 backscattering coefficients and polarimetric parameters. The results showed slightly higher separability between crops with backscattering coefficients than with polarimetric data, suggesting that backscattering coefficients better distinguish crop types. This greater separability likely contributed to the better classification results using backscattering data. These findings about the lower outputs of polarimetric parameters may be explained by the limitations of S1, which is not fully polarimetric and therefore less capable of capturing both surface and volumetric scattering from crop canopies [77]. Furthermore, the similar canopy structures of maize, soybean, and sunflower reduce the discriminative power of polarimetric data, presenting additional challenges for accurate crop classification [78].

Table 6. Comparison of the mean F1 scores all six combinations of study sites and years for classifying (a) sunflower, (b) soybean, and (c) maize using four algorithms (RF, XGBoost, MLP, InceptionTime) with the best features from S2 images, S1 backscattering coefficients, and S1 polarimetric parameters. Ind = vegetation indices, TS = time series, Back = backscattering coefficients, Polar = polarimetric parameters, Des = descending orbit, Asc = ascending orbit, Har = harmonic coefficients, Med = median features. The best algorithm/dataset combination for each crop is shown in bold case. Note: '---' indicates that the InceptionTime algorithm was not applied to the corresponding dataset (tabular datasets).

Crop Type	Classifier	S2_Ind TS	S2_Ind Med	S1_Back TS	S1_Back Med	S1_Polar Med	S2_Ind TS & S1_Back TS	S2_Ind Med & S1_Back Med	S2_Ind Med & S1_Polar Med
Sunflower	RF	69.4	70.0	82.7	84.7	73.6	85.7	87.1	82.9
	XGBoost	75.3	77.1	83.2	85.6	74.1	87.4	89.9	83.7
	MLP	74.9	75.9	82.3	82.7	67.2	84.9	89.2	78.6
	InceptionTime	82.7	---	87.2	---	---	**90.6**	---	---
Soybean	RF	60.4	63.1	46.3	51.6	25.3	61.6	65.1	52.3
	XGBoost	67.8	72.8	46.9	58.3	30.9	72.0	69.8	65.0
	MLP	71.1	69.4	49.3	62.7	28.7	71.2	75.0	66.0
	InceptionTime	83.5	---	63.6	---	---	**86.1**	---	---
Maize	RF	87.9	87.1	69.0	65.4	65.7	88.0	88.1	81.6
	XGBoost	90.0	90.1	66.0	71.2	65.0	89.7	91.1	87.6
	MLP	89.4	88.4	58.3	68.8	56.7	89.6	89.7	81.8
	InceptionTime	91.9	---	81.7	---	---	**93.5**	---	---

S2 vegetation indices and S1 backscattering coefficients were chosen for further discussion due to their superior performance over S2 spectral bands and polarimetric parameters, respectively. As shown in Table 6, the quality of the mapping of each crop depends on the sensor type (optical or SAR). For sunflower, S1 data alone (both backscattering coefficients time series and phenological features), outperformed the S2 data. However, the combination of S1 and S2 data yielded the best results for sunflower mapping. In contrast, for

soybean and maize, S2 data alone (both vegetation indices time series and phenological features) performed better than the corresponding S1 data alone—a finding consistent with previous studies [5,21]. For these two crops, the combination of S1 and S2 data also outperformed individual data sources. The superior performance of S1 for sunflower is linked to its directional behavior during peak flowering in July and August, unlike maize and soybean [17,79]. This behavior improves sunflower detection, particularly in the descending orbit (morning pass in France). During peak flowering, the vertical stem and horizontal leaf structure of young sunflowers face east in the morning, aligning with the descending pass, and westward in the evening, aligning with the ascending pass (in France). Once flowering is complete, sunflower heads permanently face east, enhancing detection with descending orbit data [12,17]. Regarding soybean and maize, Huang et al. [37] suggest that the lower water content in soybean during the growing season increases separability using optical data, as several optical bands and vegetation indices are sensitive to canopy water content. Meanwhile, Yin et al. [80] attribute this separability to maize maturing earlier than soybean.

In addition, the use of median features and harmonic coefficients alone, calculated from S2 vegetation indices, yielded similar classification results (Figure 6). Combining both harmonic coefficients and median features did not lead to any improvement. For sunflower and maize, no significant differences were observed between S2 time series and the extracted features. However, for soybean, using median features resulted in a 5% increase in the F1 score. Comparing the classification results using S2 vegetation indices time series with the extracted phenological features, the most successful set for mapping all three crops (sunflower, soybean, and maize) was the median features using XGBoost, with mean F1 scores of 77.1% for sunflower, 72.8% for soybean, and 90.1% for maize. When using S1 data, median features consistently outperformed harmonic coefficients across all three crops (Figures 8 and 9). Combining harmonic coefficients with median features did not improve results for sunflower and soybean, but for maize, this combination actually decreased the F1 score by 6.2%. Comparing the classification result using S1 backscattering coefficients time series with the extracted phenological features, the most successful set for mapping sunflower, soybean, and maize was the median features using XGBoost, with mean F1 scores of 85.6% for sunflower, 58.3% for soybean, and 71.2% for maize. S2's classification is therefore more accurate than S1's if our aim is to map all three crops together. For individual crops, the best performance for sunflower was achieved using the median features extracted from S1 backscattering coefficients (F1 score of 85.6%), for soybean using the median features extracted from S2 vegetation indices (72.8%), and for maize, both S2 vegetation indices time series and median features proved effective (both close to 90%). Based on Scharlemann et al. [81] and Qadir et al. [17], the classification performance using phenological features such as median features and harmonic coefficients is attributed to the ability of these features to capture the different phenological stages of summer crops.

However, the best approach for mapping sunflower, maize, and soybean involved using both S1 and S2 images (Table 6), with close F1 scores between median features and time series datasets (mean F1 scores of 89.9% for sunflower, 76.6% for soybean, and 91.1% for maize using median features). Within the three crops, this combination provided the greatest improvement for sunflower compared to using S2 median features alone. Previous studies have also reported higher accuracy using both S1 and S2 data, as this leverages the strengths of both sensors [5,8,10,32,39,56,82,83]. However, some studies noted varying levels of improvement depending on the crop type [84]. These findings suggest that when satellite image availability is not a concern, the choice between combined optical-SAR data or single-sensor data should depend on the crops being mapped. While combining data from both sensors can enhance classification performance across a broad range of crops, it also requires significantly more computational resources and knowledge efforts. Thus, the benefits of improved classification must be weighed against the added complexity and cost of processing [84].

The InceptionTime classifier demonstrated significant improvement over RF, XGBoost and MLP algorithms when applied to time series data. Using InceptionTime to classify the combination of S1 backscattering coefficients and S2 vegetation indices time series, the highest F1 scores were achieved for all three crops: a mean F1 score of 90.6% for sunflower, 86.1% for soybean, and 93.5% for maize. However, the degree of improvement compared to XGBoost varied depending on the crop and input data. For sunflower, InceptionTime provided a modest improvement of about 5%. In contrast, the most significant increase was obtained for soybean (around 14%) using S2 vegetation indices alone, S1 backscattering coefficients alone, or a combination of both S1 and S2. For maize, using InceptionTime with S2 vegetation indices time series alone or both S2 and S1 resulted in a small improvement of around 3%, but when using S1 backscattering coefficients alone, the F1 score saw an important increase of about 13%. Since SAR data are particularly valuable for crop classification in regions with frequent cloud cover [85], using InceptionTime to improve S1 images classification is beneficial for enhanced crop monitoring.

However, as XGBoost using combined S2 vegetation indices and S1 backscattering coefficients time series achieved mean F1 scores of 87.4% for sunflower, 72.0% for soy-bean, and 89.7% for maize (Figure 13). XGBoost with time series data remains a viable option for crop classification when data availability is not a concern, particularly considering the shorter training time with XGBoost compared to InceptionTime and the lower processing time for time series creation than for phenological features. While InceptionTime achieves high accuracy for time series classification, its high computational needs make it hard to use in situations with limited resources. In contrast, XGBoost provides competitive performance with substantially shorter training times, making it a viable alternative for crop classification, especially when combining S2 vegetation indices and S1 backscattering coefficients. This computational advantage is particularly relevant when fast classification and lower processing times for time series creation are prioritized over marginal accuracy gains.

An analysis of precision and recall for each crop using our four classifiers (RF, XGBoost, MLP, and InceptionTime) was performed using some optimal datasets—namely, a combination of S1 backscattering coefficients and S2 vegetation indices time series, as well as median features derived from this combination (Table 7). For sunflower, precision remained high across classifiers when using combination of S1 backscattering coefficients and S2 vegetation indices time series, with InceptionTime, XGBoost and RF achieving precision around 95%, indicating a low false positives rate. Precision for MLP was lower with 87.7%. However, recall scores for all four algorithms were lower than precision, with values between 80.2% and 87.9%, suggesting that some sunflower fields were misclassified, likely due to spectral similarity with other crops. For maize, both high precision and recall were achieved, particularly with InceptionTime (91.6% precision and 92.8% recall), indicating reliable classification with minimal false positives or false negatives. XGBoost and MLP also performed well, with precision and recall around 90%, demonstrating their robustness in identifying maize accurately. However, RF showed slightly lower precision and recall, with values close to 88%. Soybean represented the greatest classification challenge, with generally lower recall across classifiers compared to sunflower and maize. Although InceptionTime achieved the highest precision for soybean (91.8%), recall was lower than precision (79.0%), indicating the frequent misclassification of soybean fields. XGBoost also showed high precision (88.7%) but comparatively low recall (61.4%), while RF and MLP demonstrated moderate precision (75.9% and 78.5%) with low recall (53.4% and 66.7%), highlighting the difficulty in accurately distinguishing soybean.

Table 7. Mean precision and recall values for each crop type (sunflower, soybean, maize) and classifier (RF, XGBoost, MLP, InceptionTime) using the best two datasets: a combination of S1 backscattering coefficients and S2 vegetation indices time series, and median features derived from these datasets.

		Precision		Recall	
Crop Type	**Classifier**	**S2_Ind TS & S1_Back TS**	**S2_Ind Med & S1_Back Med**	**S2_Ind TS & S1_Back TS**	**S2_Ind Med & S1_Back Med**
Sunflower	RF	93.84	92.97	80.17	83.18
	XGBoost	95.05	93.32	81.71	87.10
	MLP	87.72	90.92	82.64	87.87
	InceptionTime	95.10	---	84.18	---
Soybean	RF	75.90	78.79	53.35	57.52
	XGBoost	88.68	82.52	61.37	61.69
	MLP	78.49	83.80	66.67	70.18
	InceptionTime	91.80	---	79.02	---
Maize	RF	88.16	88.88	88.97	88.35
	XGBoost	91.29	94.65	87.58	88.29
	MLP	93.88	92.29	86.18	88.03
	InceptionTime	91.60	---	92.80	---

When using median features extracted from the combined S1 and S2 data, the precision and recall scores remained close to those achieved with the time series data. However, median features generally resulted in slightly higher recall values for all three crops. This approach helps increase recall while keeping precision nearly the same.

In an additional experiment, we smoothed our S2 vegetation indices and S1 backscattering time series datasets using the Savitzky–Golay (SG) method to reduce noise by removing high-frequency components [17,86]. For SG smoothing the degree of the fitted polynomial function was set to three and the window-size parameter was set to seven [17]. The use of smoothed time series for classifying three crops resulted in only a slight improvement in the F1 score for S2 vegetation indices (around 2%). Conversely, the improvement was higher for S1 backscattering time series, with an average F1 score increase of 7% for the RF, XGBoost, and MLP classifiers. However, when the InceptionTime classifier was used, the improvement remained minimal (around 2%). This indicates that noise reduction is essential for enhancing the performance of RF, XGBoost, and MLP classifiers, particularly for S1 backscattering time series. Given that the S1 signal is influenced not only by vegetation characteristics but also by soil properties such as moisture and roughness [87], smoothing helps mitigate these interfering factors, leading to more reliable classification outcomes.

4.2. Classifiers Transferability Analysis

In this study, we evaluated the transferability performance of our classifiers across three types of transfer scenarios: spatial, temporal, and spatiotemporal domains. Transferability is crucial in crop classification due to the challenges in obtaining training data for each region and year. Unlike other land cover types, crops undergo rapid and dynamic changes, with sowing dates and growth cycle durations varying from year to year and across regions, making transfer scenarios more complex [88,89]. To further assess these challenges, we examined the classification accuracy for sunflower, soybean, and maize using different combinations of train and test datasets. Here, we focus on datasets with the highest F1 score (Figures 6–14), including S2 vegetation indices time series, a combination of S2 vegetation indices and S1 backscattering coefficients time series, median features

extracted from both S2 vegetation indices and S1 backscattering coefficients, and median features from S1 backscattering coefficients alone.

For sunflower, when using S2 vegetation indices time series alone (Figures 6 and 14), InceptionTime achieved F1 scores above 80% across all three types of transferability (spatial, temporal, and spatiotemporal). XGBoost also performed well, with F1 scores close to 80% for spatial and temporal transferability, although its performance dropped to around 65% for spatiotemporal transferability. The MLP consistently produced F1 scores around 75% across all three types of transferability, while RF achieved an F1 score close to 80% only for temporal transferability, proving ineffective for sunflower classification with spatial and spatiotemporal transfer scenarios. For soybean, InceptionTime maintained strong transferability performance, with F1 scores near 80% across all transferability types. XGBoost showed more variability, with F1 scores of around 75% and 70% for temporal and spatial transferability, respectively, but lower results for spatiotemporal transferability (60%). MLP demonstrated consistent but a slightly lower performance around 70% across all transferability types, while RF was only effective in temporal transferability, achieving near 80%. For maize, InceptionTime delivered excellent results, with F1 scores between 85% and 95% for all transferability types. Temporal transferability using RF, XGBoost, and MLP resulted in F1 scores above 90%, while other transferability types were slightly lower than temporal transferability but still close to 90%.

The combination of S2 vegetation indices and S1 backscattering coefficients time series significantly enhanced classification performance for sunflower. The F1 scores for InceptionTime and XGBoost exceeded 85% across all transferability types, and the MLP achieved scores of up to 87%. Notably, RF demonstrated the greatest improvement due to the inclusion of S1 data (the F1 score higher than 77%). For soybean, the addition of S1 backscattering did not significantly improve InceptionTime and MLP performance, though InceptionTime still maintained an F1 score near 80% same as its achievement using S2 vegetation indices time series. However, RF and XGBoost saw improvements in temporal transferability. For maize, the inclusion of S1 data did not significantly enhance transfer scenarios accuracy using all four algorithms, as S2 data alone yielded consistently high F1 scores across all transferability types.

Although the combination of S1 and S2 data improved transfer results, the added value of S1 backscattering coefficients is crop-dependent, with sunflower benefiting the most due to its distinct directional behavior [17]. When comparing the transferability of classifiers, InceptionTime consistently delivered stable and high results across all transferability types for all three crops, making it a strong candidate for diverse transferability scenarios. For example, in spatiotemporal transferability—the most complex type—IT achieved F1 scores close to 90% for sunflower, 80% for soybean, and 95% for maize. The robustness of InceptionTime in crop transfer scenarios has been confirmed in previous studies [63,64]. These F1 scores closely align with the results of Pandžić et al. [90], who reported F1 scores of approximately 92% for sunflower, 85% for soybean, and 90% for maize using a convolutional neural network (CNN). However, lower results have also been reported with deep learning models; for example, Che et al. [24] reported F1 scores below 90% for maize, sunflower, and soybean in spatiotemporal transferability when using a deep learning method, which comprises three modules, DeepLabV3+, channel self-attention, and histogram matching (DSH) with S2 time series data. Zhao et al. [91] evaluated the accuracy of mapping seven crop types—greenhouse vegetables, summer maize, cotton, chili, common yam rhizome, fruit trees, and forests—using S2 data. They compared the performance of five models: 1D CNN, LSTM, GRU, LSTM-CNN, and GRU-CNN. While 1D CNN achieved high overall accuracy (exceeding 85%) and outperformed LSTM and GRU individually, the hybrid models (LSTM-CNN and GRU-CNN) produced similar accuracy to the 1D CNN. In another study, Rusňák et al. [92] examined temporal transferability by applying SVM and Neural Network (NN) algorithms to map seven crops—barley, rapeseed, maize, wheat, sugar beet, sunflower, and soybean. They reported overall accuracies ranging from 84.4% to 88.9% for SVM and from 81.1% to 91.9% for NN.

Unlike the previous time series dataset, where InceptionTime was applied, the transfer scenarios using median features derived from the combination of S2 vegetation indices and S1 backscattering coefficients involved only tabular classifiers (RF, XGBoost, and MLP). All three algorithms achieved F1 scores exceeding 85% for sunflower across all transferability types, with temporal transferability showing slightly better results. Notably, these median features significantly enhanced spatiotemporal transferability for sunflower mapping, outperforming the results obtained from the time series data discussed earlier. For soybean, all classifiers achieved an F1 score of approximately 80% for temporal transferability. In spatial and spatiotemporal transferability, XGBoost and MLP gave the maximum F1 scores close to 75%, representing an improvement over time series data, although RF continued to underperform in these contexts. For maize, all classifiers consistently produced high F1 scores (above 90%) across all transferability types. However, for maize, the results did not surpass those achieved using S2 time series alone or in combination with S1 time series data.

Using median features from S1 backscattering coefficients alone, all three types of transfer scenarios for sunflower yielded F1 scores above 85% across all classifiers. For soybean, temporal transfer scenario was the only scenario that produced acceptable results across all classifiers, with F1 scores ranging from 75% to 85%. However, spatial and spatiotemporal transfer scenarios did not perform well. For maize, temporal transfer scenarios yielded strong results across all classifiers (90–95%), but spatial and spatiotemporal transfer scenarios showed lower results.

4.3. Misclassification in Crop Mapping

Misclassification in crop mapping can arise from various sources, potentially affecting the accuracy of classification. Key factors contributing to misclassification include the classifiers used [24,39], and spectral similarities between crops in satellite imagery [17,93]. In addition, environmental variation between the training and test study sites, which can result in different crop growth cycles, is critical for transfer scenarios [12,25,39]. Field size also plays a significant role in misclassification [12,64].

Concerning model-based misclassification, we evaluated four algorithms: two neural networks and two decision tree models. Among these, InceptionTime consistently showed the highest performance and stability across all three types of transfer scenarios. InceptionTime is a time series classification algorithm based on convolutional neural networks (CNN), designed to effectively handle sequential data. By using convolutional layers, InceptionTime extracts meaningful features through sliding filters, allowing it to capture temporal patterns, transitions, and dependencies within the time series data [69]. This makes InceptionTime particularly robust to temporal shifts, a key advantage in time series classification [69].

Another source of misclassification in crop identification is the spectral similarity between summer crops [94]. Figure 15a,b show the confusion matrices for the classification of S2 vegetation indices and S1 backscattering coefficients, using InceptionTime and XGBoost. These models were trained on Dijon 2020 data and tested on Tarbes 2021 data. In the confusion matrices, the rows represent the true classes while the columns indicate the predicted classes. Comparing the misclassifications among the three crops, InceptionTime results show that 21.0% of sunflower was misclassified as other crops, but only about 1% was misclassified as soybean or maize. With XGBoost, 25.1% of sunflower was misclassified as "Other crops", while 4.2% was misclassified as soybean and 0.8% as maize. For soybean, InceptionTime misclassified 18.9% as "Other crops", and around 2% as either sunflower or maize. XGBoost showed 24.2% misclassification as other crops, 1.2% as sunflower, and 2.7% as maize. For maize also, misclassifications as "Other crops" were higher than with sunflower or soybean, with 7.9% in InceptionTime and 5.4% in XGBoost. The misclassification of maize with soybean and sunflower was close to 1% and 0%, respectively. The misclassification due to the spectral similarity among summer crops can be attributed to overlapping spectral signatures before maturation [5,17,21].

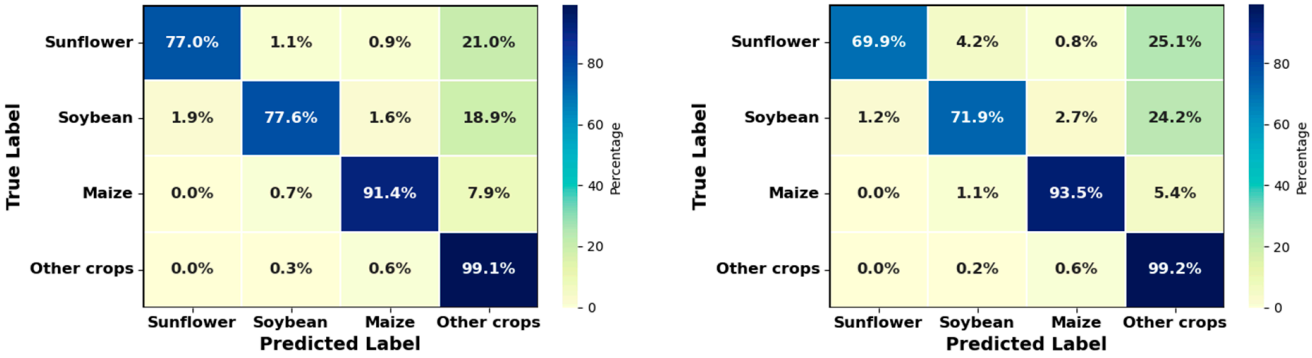

Figure 15. The confusion matrices for the classification of S2 vegetation indices and S1 backscattering coefficients, using (**a**) InceptionTime and (**b**) XGBoost (train: Dijon 2020; test: Tarbes 2021).

The shift in crop growth cycles due to environmental variations between training and test datasets also plays a crucial role in misclassification [25]. Analyzing the NDVI behavior for the three crops across the study sites and years (Figure 16a–c) revealed that all crops experienced a shorter growth period in Dijon compared to Tarbes. This shorter growth period, particularly for soybeans, was particularly evident in the VH polarization (Figure 16d–f), which is sensitive to vegetation cover, biomass, and geometric structure [95]. In our spatial transferability results, the classification of soybeans yielded lower F1 scores (Figures 6–14), which can be attributed to these differences between the study sites. Also, the peak NDVI for all three crops in Tarbes occurs about a month later than in Dijon. This delay further complicates spatial transferability between the two locations.

Field size emerged as another significant factor contributing to misclassification. Our analysis of false negatives from the classification of S2 vegetation indices and S1 backscatter coefficients to map Tarbes 2020, using the Tarbes 2021 training data with InceptionTime and XGBoost, showed that about 50% of the misclassified sunflower and soybean fields and 60% of the maize fields were smaller than 1 ha. Similarly, for XGBoost, around 40% of sunflower and soybean fields and 50% of maize fields were smaller than 1 ha. This suggests that a significant proportion of the misclassification is due to the small size of the fields, which is related to the spatial resolution limitations of the Sentinel imagery [12].

4.4. Implications and Constraints

Our results on the effectiveness of S1 and S2 data, combined with robust classifiers like XGBoost and InceptionTime, demonstrate significant applications in precision agriculture, environmental monitoring, and food security. These tools enable timely and accurate crop type mapping and monitoring. The necessity of such findings has been proven by previous studies [7,27]. Additionally, integrating SAR and optical data improves monitoring reliability, especially in regions with frequent cloud cover. This combination is useful for large-scale agricultural activities. Our findings are relevant not only for the France area but they also have potential scalability to other regions. As our results and previous studies have demonstrated, transfer generalization between different study sites is possible [90,92]. Applying classifier transferability across regions and time frames offers a scalable and cost-effective solution for crop monitoring, addressing the limitations of ground data availability. Furthermore, the adaptable framework of integrating S1 and S2 data with machine learning classifiers could be extended to other crops.

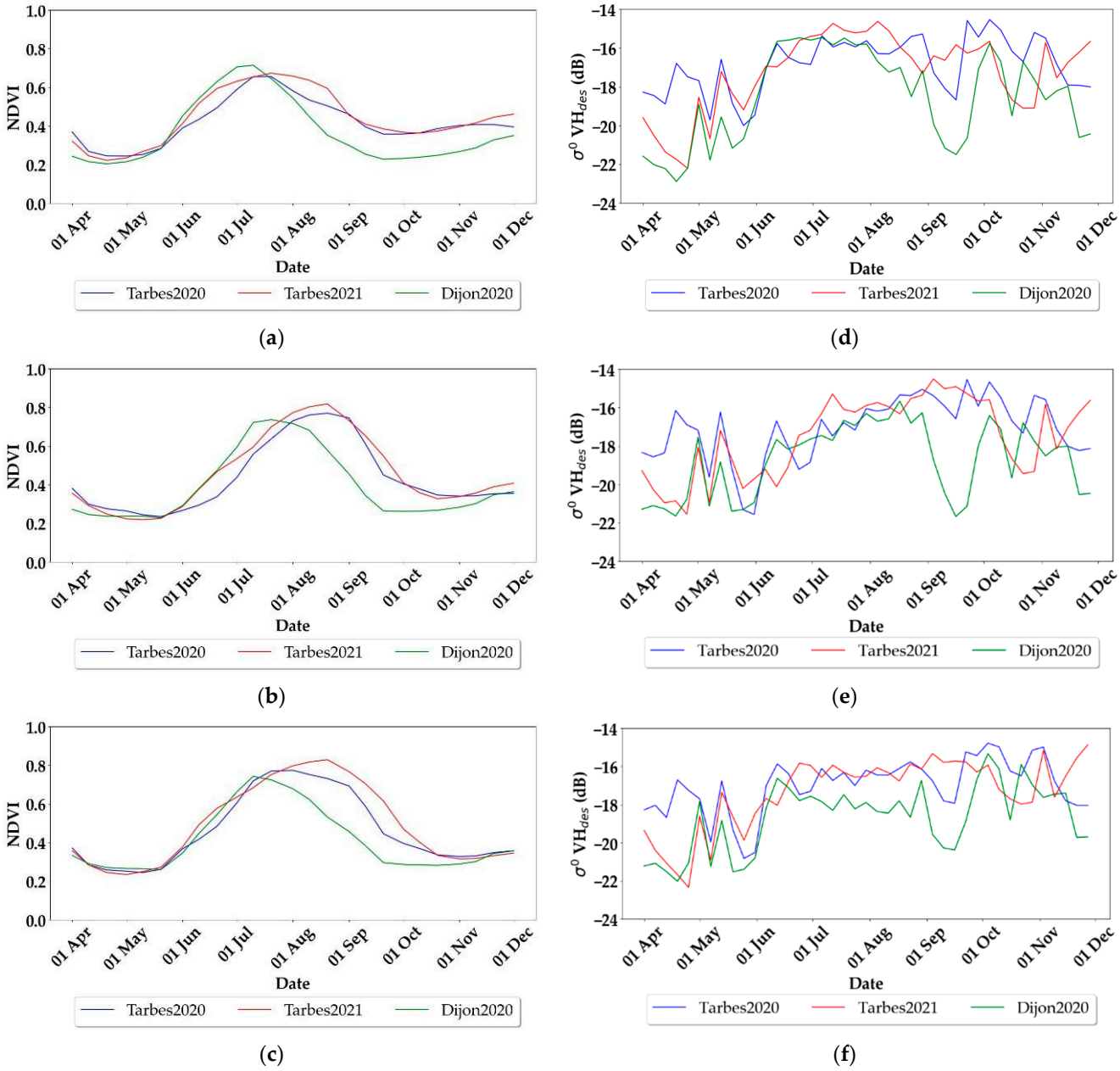

Figure 16. Temporal dynamics of NDVI and VH backscattering coefficients in three study sites and years. (**a**) NDVI sunflower, (**b**) NDVI soybean, (**c**) NDVI maize, (**d**) VH sunflower, (**e**) VH soybean, and (**f**) VH maize. The graphs display the mean values of all fields for each crop.

The limitations of this study include some challenges with machine learning models like InceptionTime, which can be sensitive to data imbalances and may favor more represented classes, leading to potential biases in predictions. Deep learning models are also "black boxes", making them hard to explain and to understand which features drive the final decision. Additionally, InceptionTime requires substantial computational resources, especially for training on large satellite datasets, which could be a challenge for scaling or using the model in low-resource settings. The satellite data itself also presents challenges. For example, S2 images can be affected by cloud cover, limiting image availability in some areas or seasons. On the other hand, S1 images, which are less weather-dependent, generally have lower accuracy than S2.

5. Conclusions

To identify the effective dataset for mapping sunflower, soybean, and maize, we compared the classification accuracy using S2 and S1 time series datasets alongside the extracted phenological features, specifically harmonic coefficients and temporal medians. We employed RF, MLP, and XGBoost classifiers across various dataset scenarios, training and testing them on different combinations of study sites and years. Additionally, the InceptionTime classifier, specifically designed for time series data, was tested exclusively with time series datasets to compare its performance against the three general machine learning algorithms (RF, XGBoost, and MLP).

Our results indicated that XGBoost outperformed RF and MLP, demonstrating its superiority due to its ability to correct residual errors and incorporate regularization. The best dataset for mapping sunflower, maize, and soybean was a combination of S1 backscattering coefficients and S2 vegetation indices, yielding similar results for phenological features and time series data (with mean F1 scores of 89.9% for sunflower, 76.6% for soybean, and 91.1% for maize). Using this combined dataset (S1 and S2), the mean F1 scores for all three types of transferability (spatial, temporal, and spatiotemporal) were comparable between the median features and time series datasets, except for the spatiotemporal transfer scenario of soybean, where the time series dataset had an F1 score 5% lower than the median features. The best individual datasets for each crop were: for sunflower, median features extracted from S1 backscattering coefficients (mean F1 score of 85.6%); for soybean, median features extracted from S2 vegetation indices (mean F1 score of 72.8%); and for maize, both S2 vegetation indices time series and median features provided an F1 score close to 90%. The choice between single-sensor and multi-sensor data should depend on the study's goal, crop, and available computational resources. While combining S1 and S2 data improves classification accuracy, it also makes the process more complicated and requires more computational resources.

The InceptionTime classifier improved classification results over XGBoost for all crops using time series data, with varying degrees of enhancement depending on the crop and input data. The highest mean F1 scores of 90.6% for sunflower, 86.0% for soybean, and 93.5% for maize were obtained using both S1 backscattering coefficients and S2 vegetation indices. For sunflower, the improvement of the mean F1 score was about 5%, while for soybean, InceptionTime boosted the mean F1 scores about 14% when classifying the optimal datasets (using S2 vegetation indices alone or S1 backscattering coefficients alone or a combination of both). For maize, improvement was 13% using S1 backscattering coefficients. These findings highlight the value of advanced time series classifiers for crop mapping, particularly in regions with frequent cloud cover.

The key findings from this study can be summarized as follows:

Classifier performance: XGBoost consistently outperformed RF and MLP in classification accuracy across various scenarios. The InceptionTime classifier, which is specifically designed for time series data, further improved classification accuracy beyond that of XGBoost. However, InceptionTime requires substantial computation time.

Optimal datasets: Using InceptionTime, the combination of S1 backscattering coefficients and S2 vegetation indices time series produced the best results. With XGBoost, median features derived from a combination of S1 backscattering coefficients and S2 vegetation indices provided slightly better results than time series data for mapping the three summer crops.

Single-sensor vs. multi-sensor data: For each crop, certain single-sensor datasets also proved effective, such as S1 median features for sunflower, S2 median features for soybean, and S2 vegetation indices time series for maize. Therefore, using multi-sensor data are not essential when the objective is to identify each class separately. However, multi-sensor data are necessary to achieve high-quality classification across all three crops together.

Comparison of S2 bands, indices, and S1 backscattering and polarimetric data: S2 indices provided the best results, while polarimetric parameters yielded lower accuracy.

Efficient mapping with limited ground data: The study demonstrated that temporal, spatial and spatiotemporal transferability approaches can be effectively applied in crop classification.

This research enhances the understanding of how different satellite data sources (S1 and S2) and machine learning classifiers can improve the mapping and monitoring of important summer crops. This has significant implications for agriculture, particularly in areas with frequent cloud cover, where large-scale, real-time crop monitoring is crucial for precision agriculture, crop yield forecasting, and food security. Future studies could explore the integration of other deep learning algorithms to further boost classification accuracy for challenging crops such as soybean and maize. In addition, conducting more detailed case studies across diverse agricultural landscapes would provide valuable insights into the transferability of classifiers, assessing how well the models generalize across regions with varying climatic conditions and crop management practices. Investigating the scalability of these findings across various regions and with reduced training data will be crucial for broadening the general applicability of this approach.

Author Contributions: Conceptualization, N.B.; methodology, N.B.; software, S.M. and C.F.D.; formal analysis, S.M. and C.F.D.; data curation, S.M., N.B., Y.N. and S.N.; writing—original draft, S.M. and N.B.; review and editing, S.M., N.B., H.B., C.F.D., D.I., S.N. and Y.N.; visualization, S.M.; supervision, N.B.; project administration, N.B. All authors have read and agreed to the published version of the manuscript.

Funding: This research was funded by the French Space Study Center (CNES, TOSCA 2024 project) and the National Research Institute for Agriculture, Food, and the Environment (INRAE).

Data Availability Statement: The data presented in this study are available on request from the corresponding author.

Acknowledgments: The authors would like to thank the French Space Study Center (CNES, TOSCA 2024), and the National Research Institute for Agriculture, Food, and the Environment (INRAE) for their support in carrying out this research. We are also grateful to the European Space Agency (ESA) for providing the S1 and S2 images.

Conflicts of Interest: The authors declare no conflicts of interest.

Appendix A. The Equations for the Accuracy Metrics

- Precision (P) measures the accuracy of positive predictions, indicating how many of the predicted positive cases are actually correct:

$$P = \frac{TP}{TP + FP}$$

- Recall evaluates how well the model identifies positive cases, showing the proportion of actual positives that were correctly classified:

$$R = \frac{TP}{TP + FN}$$

- F1-Score is the harmonic mean of Precision and Recall. It provides a single score that balances the two metrics. A high F1-Score suggests both high Precision and Recall:

$$F1 = \frac{2 \times P \times R}{P + R}$$

True Positives (TP) is the number of positive samples correctly classified as positive.
False Positives (FP) is the number of negative samples incorrectly classified as positive.
False Negatives (FN) is the number of positive samples incorrectly classified as negative.
True Negatives (TN) is the number of negative samples correctly classified as negative.

Appendix B. RF Feature Importance Analysis for Mapping Sunflower, Soybean and Maize in Tarbes 2021

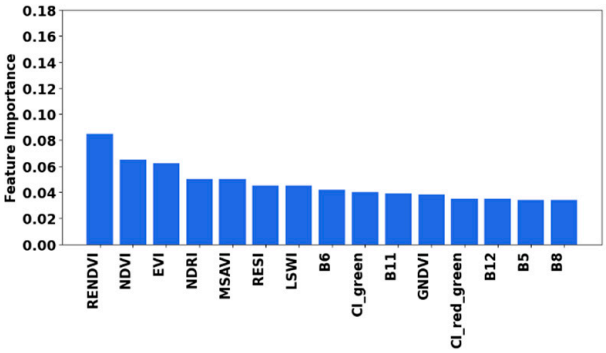

Figure A1. Features with the top 75% importance, as determined by the RF feature importance analysis, for classification of sunflower, soybean, and maize in Tarbes 2021, using 12 S2 spectral bands and 13 vegetation indices.

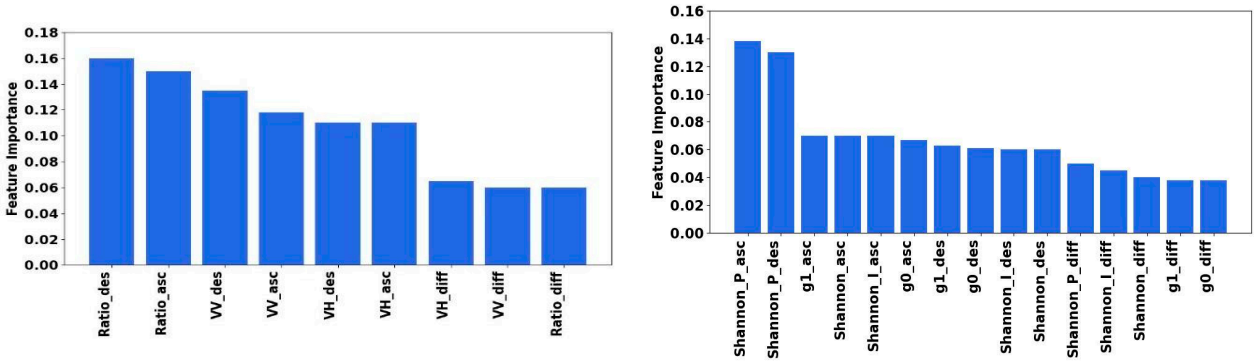

(**a**) (**b**)

Figure A2. RF feature importance analysis (top 75% importance) for classification of sunflower, soybean and maize in Tarbes 2021 using S1 images: (**a**) S1 backscattering coefficients, (**b**) S1 polarimetric parameters.

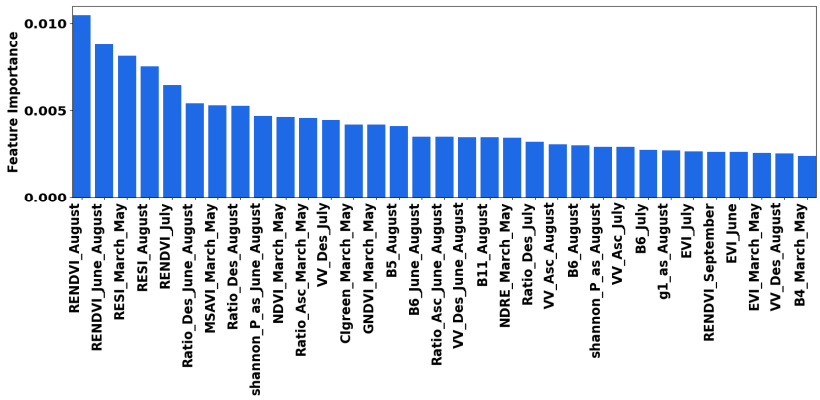

Figure A3. RF feature importance analysis (top 20% importance) for classification of sunflower, soybean and maize in Tarbes 2021 using the median features extracted from 12 S2 spectral bands, 13 vegetation indices, S1 backscattering coefficients, S1 polarimetric parameters.

References

1. Skakun, S.; Kussul, N.; Shelestov, A.Y.; Lavreniuk, M.; Kussul, O. Efficiency Assessment of Multitemporal C-Band Radarsat-2 Intensity and Landsat-8 Surface Reflectance Satellite Imagery for Crop Classification in Ukraine. *IEEE J. Sel. Top. Appl. Earth Obs. Remote Sens.* **2016**, *9*, 3712–3719. [CrossRef]
2. Conrad, C.; Dech, S.; Dubovyk, O.; Fritsch, S.; Klein, D.; Löw, F.; Schorcht, G.; Zeidler, J. Derivation of Temporal Windows for Accurate Crop Discrimination in Heterogeneous Croplands of Uzbekistan Using Multitemporal RapidEye Images. *Comput. Electron. Agric.* **2014**, *103*, 63–74. [CrossRef]
3. He, Y.; Dong, J.; Liao, X.; Sun, L.; Wang, Z.; You, N.; Li, Z.; Fu, P. Examining Rice Distribution and Cropping Intensity in a Mixed Single- and Double-Cropping Region in South China Using All Available Sentinel 1/2 Images. *Int. J. Appl. Earth Obs. Geoinf.* **2021**, *101*, 102351. [CrossRef]
4. Shayanmehr, S.; Porhajašová, J.I.; Babošová, M.; Sabouhi Sabouni, M.; Mohammadi, H.; Rastegari Henneberry, S.; Shahnoushi Foroushani, N. The Impacts of Climate Change on Water Resources and Crop Production in an Arid Region. *Agriculture* **2022**, *12*, 1056. [CrossRef]
5. Song, X.-P.; Huang, W.; Hansen, M.C.; Potapov, P. An Evaluation of Landsat, Sentinel-2, Sentinel-1 and MODIS Data for Crop Type Mapping. *Sci. Remote Sens.* **2021**, *3*, 100018. [CrossRef]
6. Rolle, M.; Tamea, S.; Claps, P.; Ayari, E.; Baghdadi, N.; Zribi, M. Analysis of Maize Sowing Periods and Cycle Phases Using Sentinel 1&2 Data Synergy. *Remote Sens.* **2022**, *14*, 3712. [CrossRef]
7. Veloso, A.; Mermoz, S.; Bouvet, A.; Le Toan, T.; Planells, M.; Dejoux, J.-F.; Ceschia, E. Understanding the Temporal Behavior of Crops Using Sentinel-1 and Sentinel-2-like Data for Agricultural Applications. *Remote Sens. Environ.* **2017**, *199*, 415–426. [CrossRef]
8. Valero, S.; Arnaud, L.; Planells, M.; Ceschia, E. Synergy of Sentinel-1 and Sentinel-2 Imagery for Early Seasonal Agricultural Crop Mapping. *Remote Sens.* **2021**, *13*, 4891. [CrossRef]
9. Han, J.; Zhang, Z.; Cao, J. Developing a New Method to Identify Flowering Dynamics of Rapeseed Using Landsat 8 and Sentinel-1/2. *Remote Sens.* **2021**, *13*, 105. [CrossRef]
10. Bazzi, H.; Baghdadi, N.; Amin, G.; Fayad, I.; Zribi, M.; Demarez, V.; Belhouchette, H. An Operational Framework for Mapping Irrigated Areas at Plot Scale Using Sentinel-1 and Sentinel-2 Data. *Remote Sens.* **2021**, *13*, 2584. [CrossRef]
11. Dong, J.; Xiao, X.; Kou, W.; Qin, Y.; Zhang, G.; Li, L.; Jin, C.; Zhou, Y.; Wang, J.; Biradar, C.; et al. Tracking the Dynamics of Paddy Rice Planting Area in 1986–2010 through Time Series Landsat Images and Phenology-Based Algorithms. *Remote Sens. Environ.* **2015**, *160*, 99–113. [CrossRef]
12. Qadir, A.; Skakun, S.; Kussul, N.; Shelestov, A.; Becker-Reshef, I. A Generalized Model for Mapping Sunflower Areas Using Sentinel-1 SAR Data. *Remote Sens. Environ.* **2024**, *306*, 114132. [CrossRef]
13. Vali, A.; Comai, S.; Matteucci, M. Deep Learning for Land Use and Land Cover Classification Based on Hyperspectral and Multispectral Earth Observation Data: A Review. *Remote Sens.* **2020**, *12*, 2495. [CrossRef]
14. Mercier, A.; Betbeder, J.; Rumiano, F.; Baudry, J.; Gond, V.; Blanc, L.; Bourgoin, C.; Cornu, G.; Ciudad, C.; Marchamalo, M.; et al. Evaluation of Sentinel-1 and 2 Time Series for Land Cover Classification of Forest–Agriculture Mosaics in Temperate and Tropical Landscapes. *Remote Sens.* **2019**, *11*, 979. [CrossRef]
15. Woźniak, E.; Rybicki, M.; Kofman, W.; Aleksandrowicz, S.; Wojtkowski, C.; Lewiński, S.; Bojanowski, J.; Musiał, J.; Milewski, T.; Slesiński, P.; et al. Multi-Temporal Phenological Indices Derived from Time Series Sentinel-1 Images to Country-Wide Crop Classification. *Int. J. Appl. Earth Obs. Geoinf.* **2022**, *107*, 102683. [CrossRef]
16. Nasrallah, A.; Baghdadi, N.; El Hajj, M.; Darwish, T.; Belhouchette, H.; Faour, G.; Darwich, S.; Mhawej, M. Sentinel-1 Data for Winter Wheat Phenology Monitoring and Mapping. *Remote Sens.* **2019**, *11*, 2228. [CrossRef]
17. Qadir, A.; Skakun, S.; Eun, J.; Prashnani, M.; Shumilo, L. Sentinel-1 Time Series Data for Sunflower (Helianthus Annuus) Phenology Monitoring. *Remote Sens. Environ.* **2023**, *295*, 113689. [CrossRef]
18. Ioannidou, M.; Koukos, A.; Sitokonstantinou, V.; Papoutsis, I.; Kontoes, C. Assessing the Added Value of Sentinel-1 PolSAR Data for Crop Classification. *Remote Sens.* **2022**, *14*, 5739. [CrossRef]
19. Wang, M.; Wang, L.; Guo, Y.; Cui, Y.; Liu, J.; Chen, L.; Wang, T.; Li, H. A Comprehensive Evaluation of Dual-Polarimetric Sentinel-1 SAR Data for Monitoring Key Phenological Stages of Winter Wheat. *Remote Sens.* **2024**, *16*, 1659. [CrossRef]
20. Zhang, H.; Kang, J.; Xu, X.; Zhang, L. Accessing the Temporal and Spectral Features in Crop Type Mapping Using Multi-Temporal Sentinel-2 Imagery: A Case Study of Yi'an County, Heilongjiang Province, China. *Comput. Electron. Agric.* **2020**, *176*, 105618. [CrossRef]
21. Cai, Y.; Guan, K.; Peng, J.; Wang, S.; Seifert, C.; Wardlow, B.; Li, Z. A High-Performance and in-Season Classification System of Field-Level Crop Types Using Time-Series Landsat Data and a Machine Learning Approach. *Remote Sens. Environ.* **2018**, *210*, 35–47. [CrossRef]
22. Wang, Q.; Yang, B.; Li, L.; Liang, H.; Zhu, X.; Cao, R. Within-Season Crop Identification by the Fusion of Spectral Time-Series Data and Historical Crop Planting Data. *Remote Sens.* **2023**, *15*, 5043. [CrossRef]
23. Hamidi, M.; Homayouni, S.; Safari, A.; Hasani, H. Deep Learning Based Crop-Type Mapping Using SAR and Optical Data Fusion. *Int. J. Appl. Earth Obs. Geoinf.* **2024**, *129*, 103860. [CrossRef]
24. Che, H.; Pan, Y.; Xia, X.; Zhu, X.; Li, L.; Huang, Y.; Zheng, X.; Wang, L. A New Transferable Deep Learning Approach for Crop Mapping. *GIsci Remote Sens.* **2024**, *61*, 2395700. [CrossRef]

25. Tiwari, V.; Tulbure, M.G.; Caineta, J.; Gaines, M.D.; Perin, V.; Kamal, M.; Krupnik, T.J.; Aziz, M.A.; Islam, A.T. Automated In-Season Rice Crop Mapping Using Sentinel Time-Series Data and Google Earth Engine: A Case Study in Climate-Risk Prone Bangladesh. *J. Environ. Manag.* **2024**, *351*, 119615. [CrossRef] [PubMed]
26. Al-Shammari, D.; Fuentes, I.; Whelan, B.M.; Wang, C.; Filippi, P.; Bishop, T.F.A. Combining Sentinel 1, Sentinel 2 and MODIS Data for Major Winter Crop Type Classification over the Murray Darling Basin in Australia. *Remote Sens. Appl.* **2024**, *34*, 101200. [CrossRef]
27. Demarez, V.; Helen, F.; Marais-Sicre, C.; Baup, F. In-Season Mapping of Irrigated Crops Using Landsat 8 and Sentinel-1 Time Series. *Remote Sens.* **2019**, *11*, 118. [CrossRef]
28. Wang, S.; Di Tommaso, S.; Deines, J.M.; Lobell, D.B. Mapping Twenty Years of Corn and Soybean across the US Midwest Using the Landsat Archive. *Sci. Data* **2020**, *7*, 307. [CrossRef]
29. Wang, D.; Cao, W.; Zhang, F.; Li, Z.; Xu, S.; Wu, X. A Review of Deep Learning in Multiscale Agricultural Sensing. *Remote Sens.* **2022**, *14*, 559. [CrossRef]
30. Zhong, L.; Hu, L.; Zhou, H. Deep Learning Based Multi-Temporal Crop Classification. *Remote Sens. Environ.* **2019**, *221*, 430–443. [CrossRef]
31. Campos-Taberner, M.; García-Haro, F.J.; Martínez, B.; Izquierdo-Verdiguier, E.; Atzberger, C.; Camps-Valls, G.; Gilabert, M.A. Understanding Deep Learning in Land Use Classification Based on Sentinel-2 Time Series. *Sci. Rep.* **2020**, *10*, 17188. [CrossRef] [PubMed]
32. Ienco, D.; Interdonato, R.; Gaetano, R.; Ho Tong Minh, D. Combining Sentinel-1 and Sentinel-2 Satellite Image Time Series for Land Cover Mapping via a Multi-Source Deep Learning Architecture. *ISPRS J. Photogramm. Remote Sens.* **2019**, *158*, 11–22. [CrossRef]
33. Zhang, C.; Sargent, I.; Pan, X.; Li, H.; Gardiner, A.; Hare, J.; Atkinson, P.M. Joint Deep Learning for Land Cover and Land Use Classification. *Remote Sens. Environ.* **2019**, *221*, 173–187. [CrossRef]
34. USDA. Available online: https://Fas.Usda.Gov/Data/Production/Commodity/0440000 (accessed on 15 January 2024).
35. Eurostat. Available online: https://ec.europa.eu/eurostat/statistics-explained/index.php?title=Main_Page (accessed on 14 November 2024).
36. Statista. Available online: https://Www.Statista.Com/Statistics/263937/Vegetable-Oils-Global-Consumption/ (accessed on 1 September 2024).
37. Huang, Y.; Qiu, B.; Chen, C.; Zhu, X.; Wu, W.; Jiang, F.; Lin, D.; Peng, Y. Automated Soybean Mapping Based on Canopy Water Content and Chlorophyll Content Using Sentinel-2 Images. *Int. J. Appl. Earth Obs. Geoinf.* **2022**, *109*, 102801. [CrossRef]
38. Song, X.-P.; Potapov, P.V.; Krylov, A.; King, L.; Di Bella, C.M.; Hudson, A.; Khan, A.; Adusei, B.; Stehman, S.V.; Hansen, M.C. National-Scale Soybean Mapping and Area Estimation in the United States Using Medium Resolution Satellite Imagery and Field Survey. *Remote Sens. Environ.* **2017**, *190*, 383–395. [CrossRef]
39. Chen, Y.; Hou, J.; Huang, C.; Zhang, Y.; Li, X. Mapping Maize Area in Heterogeneous Agricultural Landscape with Multi-Temporal Sentinel-1 and Sentinel-2 Images Based on Random Forest. *Remote Sens.* **2021**, *13*, 2988. [CrossRef]
40. Shorachi, M.; Kumar, V.; Steele-Dunne, S.C. Sentinel-1 SAR Backscatter Response to Agricultural Drought in The Netherlands. *Remote Sens.* **2022**, *14*, 2435. [CrossRef]
41. Cai, W.; Tian, J.; Li, X.; Zhu, L.; Chen, B. A New Multiple Phenological Spectral Feature for Mapping Winter Wheat. *Remote Sens.* **2022**, *14*, 4529. [CrossRef]
42. Lin, C.; Zhong, L.; Song, X.-P.; Dong, J.; Lobell, D.B.; Jin, Z. Early- and in-Season Crop Type Mapping without Current-Year Ground Truth: Generating Labels from Historical Information via a Topology-Based Approach. *Remote Sens. Environ.* **2022**, *274*, 112994. [CrossRef]
43. Hersbach, H.; Bell, B.; Berrisford, P.; Hirahara, S.; Horányi, A.; Muñoz-Sabater, J.; Nicolas, J.; Peubey, C.; Radu, R.; Schepers, D.; et al. The ERA5 Global Reanalysis. *Q. J. R. Meteorol. Soc.* **2020**, *146*, 1999–2049. [CrossRef]
44. USDA. Rapeseed Maps. Available online: https://Ipad.Fas.Usda.Gov/Cropexplorer/Cropview/CommodityView.Aspx?Cropid=2226000&sel_year=2021&rankby=Production (accessed on 15 January 2024).
45. Gorelick, N.; Hancher, M.; Dixon, M.; Ilyushchenko, S.; Thau, D.; Moore, R. Google Earth Engine: Planetary-Scale Geospatial Analysis for Everyone. *Remote Sens. Environ.* **2017**, *202*, 18–27. [CrossRef]
46. Rouse, J.W.; Haas, R.H.; Deering, D.W. Monitoring Vegetation Systems in the Great Plains with ERTS (Earth Resources Technology Satellite). In Proceedings of the 3rd Earth Resources Technology Satellite Symposium, Greenbelt, MD, USA, 14 December 1974; pp. 309–317.
47. Xiao, X.; Hollinger, D.; Aber, J.; Goltz, M.; Davidson, E.A.; Zhang, Q.; Moore, B. Satellite-Based Modeling of Gross Primary Production in an Evergreen Needleleaf Forest. *Remote Sens. Environ.* **2004**, *89*, 519–534. [CrossRef]
48. Gitelson, A.; Merzlyak, M.N. Spectral Reflectance Changes Associated with Autumn Senescence of Aesculus Hippocastanum L. and Acer Platanoides L. Leaves. Spectral Features and Relation to Chlorophyll Estimation. *J. Plant Physiol.* **1994**, *143*, 286–292. [CrossRef]
49. Gitelson, A.A.; Merzlyak, M.N.; Lichtenthaler, H.K. Detection of Red Edge Position and Chlorophyll Content by Reflectance Measurements Near 700 Nm. *J. Plant Physiol.* **1996**, *148*, 501–508. [CrossRef]

50. Qi, J.; Marsett, R.; Heilman, P.; Bieden-bender, S.; Moran, S.; Goodrich, D.; Weltz, M. RANGES Improves Satellite-based Information and Land Cover Assessments in Southwest United States. *Eos Trans. Am. Geophys. Union.* **2002**, *83*, 601–606. [CrossRef]
51. Biard, F. Crop Residue Estimation Using Multiband Reflectance. *Remote Sens. Environ.* **1997**, *59*, 530–536. [CrossRef]
52. McFEETERS, S.K. The Use of the Normalized Difference Water Index (NDWI) in the Delineation of Open Water Features. *Int. J. Remote Sens.* **1996**, *17*, 1425–1432. [CrossRef]
53. Gitelson, A.; Merzlyak, M.N. Quantitative Estimation of Chlorophyll-a Using Reflectance Spectra: Experiments with Autumn Chestnut and Maple Leaves. *J. Photochem. Photobiol. B* **1994**, *22*, 247–252. [CrossRef]
54. Huete, A.; Justice, C.; Liu, H. Development of Vegetation and Soil Indices for MODIS-EOS. *Remote Sens. Environ.* **1994**, *49*, 224–234. [CrossRef]
55. Qi, J.; Chehbouni, A.; Huete, A.R.; Kerr, Y.H.; Sorooshian, S. A Modified Soil Adjusted Vegetation Index. *Remote Sens. Environ.* **1994**, *48*, 119–126. [CrossRef]
56. LUO, C.; LIU, H.; LU, L.; LIU, Z.; KONG, F.; ZHANG, X. Monthly Composites from Sentinel-1 and Sentinel-2 Images for Regional Major Crop Mapping with Google Earth Engine. *J. Integr. Agric.* **2021**, *20*, 1944–1957. [CrossRef]
57. Jakubauskas, M.E.; Legates, D.R.; Kastens, J.H. Crop Identification Using Harmonic Analysis of Time-Series AVHRR NDVI Data. *Comput. Electron. Agric.* **2002**, *37*, 127–139. [CrossRef]
58. Mingwei, Z.; Qingbo, Z.; Zhongxin, C.; Jia, L.; Yong, Z.; Chongfa, C. Crop Discrimination in Northern China with Double Cropping Systems Using Fourier Analysis of Time-Series MODIS Data. *Int. J. Appl. Earth Obs. Geoinf.* **2008**, *10*, 476–485. [CrossRef]
59. Jakubauskas, M.; Legates, D. Harmonic Analysis of Time-Series Avhrr Ndvi Data for Characterizing Us Great Plains Land Use/Land Cover. In Proceedings of the International Society for Photogrammetry and Remote Sensing, Amsterdam, The Netherlands, 16–23 July 2000; pp. 384–389.
60. Sun, J.; Yan, S.; Yao, X.; Gao, B.; Yang, J. A Segment Anything Model Based Weakly Supervised Learning Method for Crop Mapping Using Sentinel-2 Time Series Images. *Int. J. Appl. Earth Obs. Geoinf.* **2024**, *133*, 104085. [CrossRef]
61. Prins, A.J.; Van Niekerk, A. Crop Type Mapping Using LiDAR, Sentinel-2 and Aerial Imagery with Machine Learning Algorithms. *Geo-Spat. Inf. Sci.* **2021**, *24*, 215–227. [CrossRef]
62. He, S.; Peng, P.; Chen, Y.; Wang, X. Multi-Crop Classification Using Feature Selection-Coupled Machine Learning Classifiers Based on Spectral, Textural and Environmental Features. *Remote Sens.* **2022**, *14*, 3153. [CrossRef]
63. Maleki, S.; Baghdadi, N.; Najem, S.; Dantas, C.F.; Bazzi, H.; Ienco, D. Determining the Optimal Temporal Windows for Rapeseed Detection Using Sentinel-1 Time Series and Deep Learning. *Remote Sens.* **2024**, *16*, 549. [CrossRef]
64. Maleki, S.; Baghdadi, N.; Dantas, C.F.; Najem, S.; Bazzi, H.; Reluy, N.P.; Ienco, D.; Zribi, M. Artificial Intelligence Algorithms for Rapeseed Fields Mapping Using Sentinel-1 Time Series: Temporal Transfer Scenario and Ground Sampling Constraints. *IEEE J. Sel. Top. Appl. Earth Obs. Remote Sens.* **2023**, *16*, 8884–8899. [CrossRef]
65. Duro, D.C.; Franklin, S.E.; Dubé, M.G. Multi-Scale Object-Based Image Analysis and Feature Selection of Multi-Sensor Earth Observation Imagery Using Random Forests. *Int. J. Remote Sens.* **2012**, *33*, 4502–4526. [CrossRef]
66. Ndikumana, E.; Ho Tong Minh, D.; Baghdadi, N.; Courault, D.; Hossard, L. Deep Recurrent Neural Network for Agricultural Classification Using Multitemporal SAR Sentinel-1 for Camargue, France. *Remote Sens.* **2018**, *10*, 1217. [CrossRef]
67. Wang, L.; Wang, J.; Liu, Z.; Zhu, J.; Qin, F. Evaluation of a Deep-Learning Model for Multispectral Remote Sensing of Land Use and Crop Classification. *Crop J.* **2022**, *10*, 1435–1451. [CrossRef]
68. Xia, Y.; Jiang, S.; Meng, L.; Ju, X. XGBoost-B-GHM: An Ensemble Model with Feature Selection and GHM Loss Function Optimization for Credit Scoring. *Systems* **2024**, *12*, 254. [CrossRef]
69. Ismail Fawaz, H.; Lucas, B.; Forestier, G.; Pelletier, C.; Schmidt, D.F.; Weber, J.; Webb, G.I.; Idoumghar, L.; Muller, P.A.; Petitjean, F. InceptionTime: Finding AlexNet for Time Series Classification. *Data Min. Knowl. Discov.* **2020**, *34*, 1936–1962. [CrossRef]
70. Li, Y.; Li, M.; Li, C.; Liu, Z. Forest Aboveground Biomass Estimation Using Landsat 8 and Sentinel-1A Data with Machine Learning Algorithms. *Sci. Rep.* **2020**, *10*, 9952. [CrossRef]
71. Friedman, J.H. Stochastic Gradient Boosting. *Comput. Stat. Data Anal.* **2002**, *38*, 367–378. [CrossRef]
72. Mazzia, V.; Khaliq, A.; Chiaberge, M. Improvement in Land Cover and Crop Classification Based on Temporal Features Learning from Sentinel-2 Data Using Recurrent-Convolutional Neural Network (R-CNN). *Appl. Sci.* **2019**, *10*, 238. [CrossRef]
73. Hashemi, M.G.Z.; Tan, P.-N.; Jalilvand, E.; Wilke, B.; Alemohammad, H.; Das, N.N. Yield Estimation from SAR Data Using Patch-Based Deep Learning and Machine Learning Techniques. *Comput. Electron. Agric.* **2024**, *226*, 109340. [CrossRef]
74. Herrero-Huerta, M.; Rodriguez-Gonzalvez, P.; Rainey, K.M. Yield Prediction by Machine Learning from UAS-Based Multi-Sensor Data Fusion in Soybean. *Plant Methods* **2020**, *16*, 78. [CrossRef]
75. Sun, Y.; Hao, Z.; Chang, H.; Yang, J.; Ding, G.; Guo, Z.; He, X.; Huang, J. Accurate Mapping of Rapeseed Fields in the Initial Flowering Stage Using Sentinel-2 Satellite Images and Convolutional Neural Networks. *Ecol. Indic.* **2024**, *162*, 112027. [CrossRef]
76. Saini, R.; Ghosh, S.K. Crop Classification in a Heterogeneous Agricultural Environment Using Ensemble Classifiers and Single-Date Sentinel-2A Imagery. *Geocarto Int.* **2021**, *36*, 2141–2159. [CrossRef]
77. Ji, K.; Wu, Y. Scattering Mechanism Extraction by a Modified Cloude-Pottier Decomposition for Dual Polarization SAR. *Remote Sens.* **2015**, *7*, 7447–7470. [CrossRef]
78. Gella, G.W.; Bijker, W.; Belgiu, M. Mapping Crop Types in Complex Farming Areas Using SAR Imagery with Dynamic Time Warping. *ISPRS J. Photogramm. Remote Sens.* **2021**, *175*, 171–183. [CrossRef]

79. Atamian, H.S.; Creux, N.M.; Brown, R.I.; Garner, A.G.; Blackman, B.K.; Harmer, S.L. Circadian Regulation of Sunflower Heliotropism, Floral Orientation, and Pollinator Visits. *Science (1979)* **2016**, *353*, 587–590. [CrossRef] [PubMed]
80. Yin, H.; Prishchepov, A.V.; Kuemmerle, T.; Bleyhl, B.; Buchner, J.; Radeloff, V.C. Mapping Agricultural Land Abandonment from Spatial and Temporal Segmentation of Landsat Time Series. *Remote Sens. Environ.* **2018**, *210*, 12–24. [CrossRef]
81. Scharlemann, J.P.W.; Benz, D.; Hay, S.I.; Purse, B.V.; Tatem, A.J.; Wint, G.R.W.; Rogers, D.J. Global Data for Ecology and Epidemiology: A Novel Algorithm for Temporal Fourier Processing MODIS Data. *PLoS ONE* **2008**, *3*, e1408. [CrossRef]
82. Inglada, J.; Vincent, A.; Arias, M.; Marais-Sicre, C. Improved Early Crop Type Identification By Joint Use of High Temporal Resolution SAR And Optical Image Time Series. *Remote Sens.* **2016**, *8*, 362. [CrossRef]
83. Orusa, T.; Cammareri, D.; Borgogno Mondino, E.B. A Possible Land Cover EAGLE Approach to Overcome Remote Sensing Limitations in the Alps Based on Sentinel-1 and Sentinel-2: The Case of Aosta Valley (NW Italy). *Remote Sens.* **2022**, *15*, 178. [CrossRef]
84. Orynbaikyzy, A.; Gessner, U.; Conrad, C. Crop Type Classification Using a Combination of Optical and Radar Remote Sensing Data: A Review. *Int. J. Remote Sens.* **2019**, *40*, 6553–6595. [CrossRef]
85. Zhang, H.; Liu, W.; Zhang, L. Seamless and Automated Rapeseed Mapping for Large Cloudy Regions Using Time-Series Optical Satellite Imagery. *ISPRS J. Photogramm. Remote Sens.* **2022**, *184*, 45–62. [CrossRef]
86. Savitzky, A.; Golay, M.J.E. Smoothing and Differentiation of Data by Simplified Least Squares Procedures. *Anal. Chem.* **1964**, *36*, 1627–1639. [CrossRef]
87. Baghdadi, N.; Cerdan, O.; Zribi, M.; Auzet, V.; Darboux, F.; El Hajj, M.; Kheir, R.B. Operational Performance of Current Synthetic Aperture Radar Sensors in Mapping Soil Surface Characteristics in Agricultural Environments: Application to Hydrological and Erosion Modelling. *Hydrol. Process* **2008**, *22*, 9–20. [CrossRef]
88. Belgiu, M.; Bijker, W.; Csillik, O.; Stein, A. Phenology-Based Sample Generation for Supervised Crop Type Classification. *Int. J. Appl. Earth Obs. Geoinf.* **2021**, *95*, 102264. [CrossRef]
89. Luciano, A.C. dos S.; Picoli, M.C.A.; Rocha, J.V.; Franco, H.C.J.; Sanches, G.M.; Leal, M.R.L.V.; le Maire, G. Generalized Space-Time Classifiers for Monitoring Sugarcane Areas in Brazil. *Remote Sens. Environ.* **2018**, *215*, 438–451. [CrossRef]
90. Pandžić, M.; Pavlović, D.; Matavulj, P.; Brdar, S.; Marko, O.; Crnojević, V.; Kilibarda, M. Interseasonal Transfer Learning for Crop Mapping Using Sentinel-1 Data. *Int. J. Appl. Earth Obs. Geoinf.* **2024**, *128*, 103718. [CrossRef]
91. Zhao, H.; Duan, S.; Liu, J.; Sun, L.; Reymondin, L. Evaluation of Five Deep Learning Models for Crop Type Mapping Using Sentinel-2 Time Series Images with Missing Information. *Remote Sens.* **2021**, *13*, 2790. [CrossRef]
92. Rusňák, T.; Kasanický, T.; Malík, P.; Mojžiš, J.; Zelenka, J.; Sviček, M.; Abrahám, D.; Halabuk, A. Crop Mapping without Labels: Investigating Temporal and Spatial Transferability of Crop Classification Models Using a 5-Year Sentinel-2 Series and Machine Learning. *Remote Sens.* **2023**, *15*, 3414. [CrossRef]
93. Xie, G.; Niculescu, S. Mapping Crop Types Using Sentinel-2 Data Machine Learning and Monitoring Crop Phenology with Sentinel-1 Backscatter Time Series in Pays de Brest, Brittany, France. *Remote Sens.* **2022**, *14*, 4437. [CrossRef]
94. Peña, J.; Gutiérrez, P.; Hervás-Martínez, C.; Six, J.; Plant, R.; López-Granados, F. Object-Based Image Classification of Summer Crops with Machine Learning Methods. *Remote Sens.* **2014**, *6*, 5019–5041. [CrossRef]
95. Bazzi, H.; Baghdadi, N.; El Hajj, M.; Zribi, M. Potential of Sentinel-1 Surface Soil Moisture Product for Detecting Heavy Rainfall in the South of France. *Sensors* **2019**, *19*, 802. [CrossRef]